iScience

CellPress

Article

Ras Downstream Effector GGCT Alleviates Oncogenic Stress

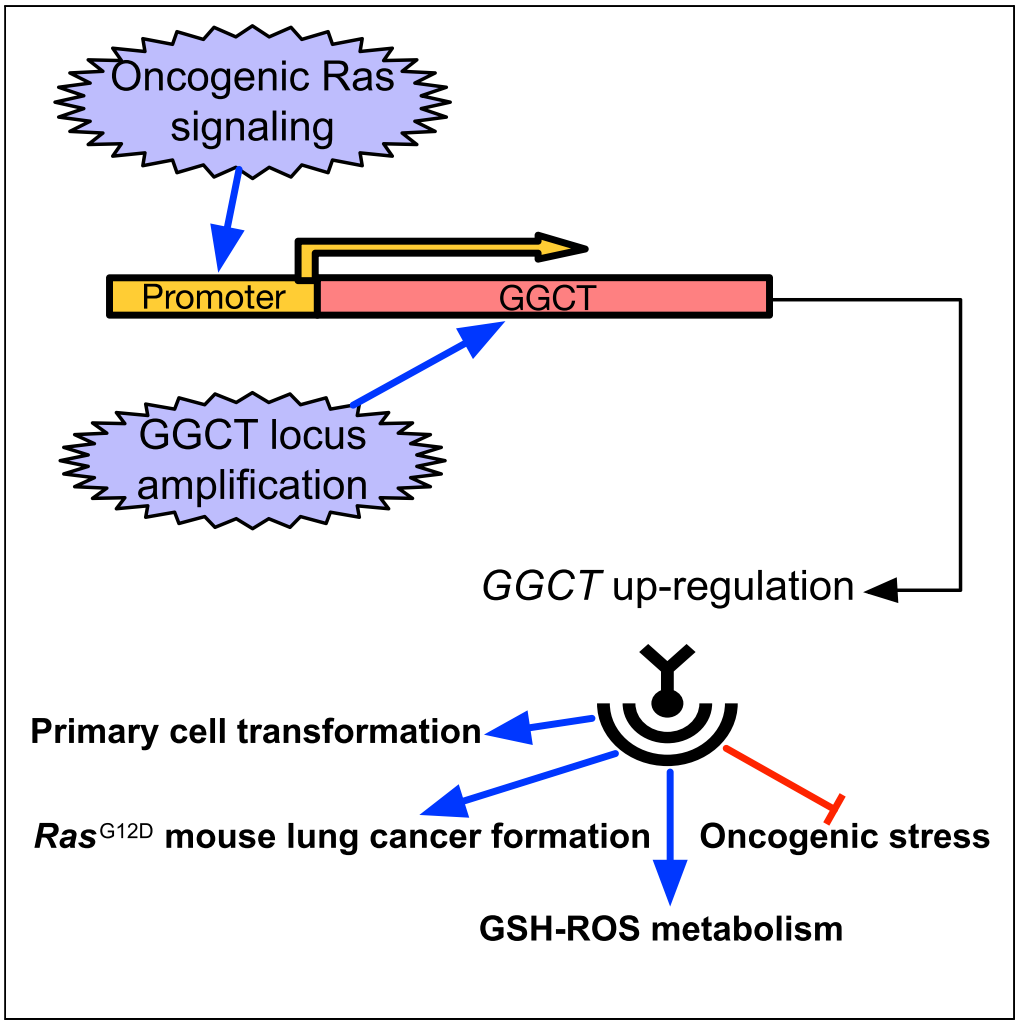

Zaoke He, Shixiang Wang, Yuanyuan Shao, ..., Junhao Hu, Feng Zhang, Xue-Song Liu

liuxs@shanghaitech.edu.cn

HIGHLIGHTS

GGCT is a target of Ras and is required for Ras-induced cancer formation

GGCT deletion is compatible with normal mouse development and tissue function

GGCT genomic locus is amplified in multiple human cancer types

GGCT could alleviate oncogenic stress by regulating GSH-ROS metabolism

He et al., iScience *19*, 256–266
September 27, 2019
https://doi.org/10.1016/j.isci.2019.07.036

iScience

CellPress

Article

Ras Downstream Effector GGCT Alleviates Oncogenic Stress

Zaoke He,[1,4,5,6] Shixiang Wang,[1,4,5,6] Yuanyuan Shao,[1,6] Jing Zhang,[1,4,5,6] Xiaolin Wu,[1] Yuxing Chen,[1] Junhao Hu,[3] Feng Zhang,[2] and Xue-Song Liu[1,7,*]

SUMMARY

How cells adapt to oncogenic transformation-associated cellular stress and become fully transformed is still unknown. Here we identified a novel GGCT-regulated glutathione (GSH)-reactive oxygen species (ROS) metabolic pathway in oncogenic stress alleviation. We identified GGCT as a target of oncogenic Ras and that it is required for oncogenic Ras-induced primary mouse cell proliferation and transformation and *in vivo* lung cancer formation in the *LSL-Kras G12D* mouse model. However, *GGCT* deficiency is compatible with normal mouse development, suggesting that GGCT can be a cancer-specific therapeutic target. Genetically amplified *GGCT* locus further supports the oncogenic driving function of GGCT. In summary, our study not only identifies an oncogenic function of GGCT but also identifies a novel regulator of GSH metabolism, with implications for further understanding of oncogenic stress and cancer treatment.

INTRODUCTION

Oncogenic transformation in primary somatic cells always leads to cellular stresses, which function as a fail-safe mechanism to prevent cancer formation (Luo et al., 2009). How cells adapt to these oncogenic stresses and become fully transformed is still not very clear. Activating Ras mutations are frequently observed in various cancers; however, these Ras mutants are known to be "undruggable" targets (Cox et al., 2014). Ras downstream targets would be surrogate drug targets for these Ras oncoproteins. Here we identified a novel oncogenic Ras downstream target GGCT, and further characterized GGCT function using mouse models, cancer genomics, and cell biochemical approaches.

GGCT was previously named C7orf24 and was originally identified as a protein up-regulated in bladder urothelial carcinoma (Kageyama et al., 2007). Subsequent studies indicated that GGCT protein or mRNA is overexpressed in multiple human cancers including breast (Gromov et al., 2010), lung, esophagus, stomach, bile duct, and uterine cervix cancer (Amano et al., 2012). In 2008, C7orf24 was identified as γ-glutamyl cyclotransferase, and this study renamed C7orf24 as GGCT (Oakley et al., 2008). The physiological function of this enzyme activity in mammals is not clear. Actually, C7orf24 is not the only protein showing this enzyme activity in mammalian cells (Chi et al., 2014). γ-Glutamyl cyclotransferase catalyzes the following reaction: γ-glutamyl-amino acid → 5-oxoproline + amino acid. This enzyme was supposed to participate in glutathione (GSH) homeostasis. Extracellular GSH can be hydrolyzed by membrane-bound γ-glutamyl transpeptidase (GGT) to cysteinylglycine and γ-glutamyl-amino acid dipeptide (Anderson, 1998; Meister, 1988). In the cytoplasm, γ-glutamyl cyclotransferase cleaves the γ-glutamyl-amino acid to give 5-oxoproline and amino acid (Meister, 1974). However, the function of GGCT (C7orf24) in GSH homeostasis is still unknown. The function of γ-glutamyl cyclotransferase enzyme activity in cancer is also unknown; association between this enzyme activity and human cancer has not been reported.

It is already known that protein and mRNA expression of *GGCT* is up-regulated in multiple types of cancers. However, it is still unknown if *GGCT* expression up-regulation is simply a by-product of cancer formation or if *GGCT* up-regulation is required for cancer evolution. The selective accumulation of genetic alterations favoring *GGCT* up-regulation in cancer, but not normal control tissues, can serve as important cancer genomic evidence supporting the cancer-driving (or oncogenic) function of *GGCT*.

Here we systematically studied human cancer genome and identified significant *GGCT* gene amplification in human lung adenocarcinoma (LUAD). *GGCT* genomic locus amplification can directly lead to *GGCT* mRNA up-regulation, suggesting a cancer-driving function of *GGCT* in human cancer. With newly generated *GGCT* knockout mouse model and primary cells, we demonstrated a critical role of GGCT in GSH

[1]School of Life Science and Technology, ShanghaiTech University, Shanghai 201203, China

[2]Core Facility, Department of Clinical Laboratory, Quzhou People's Hospital, Quzhou, Zhejiang, China

[3]Interdisciplinary Research Center on Biology and Chemistry, Shanghai Institute of Organic Chemistry, Chinese Academy of Sciences, Shanghai, China

[4]Shanghai Institute of Biochemistry and Cell Biology, Chinese Academy of Sciences, Shanghai, China

[5]University of Chinese Academy of Sciences, Beijing, China

[6]These authors contributed equally

[7]Lead Contact

*Correspondence: liuxs@shanghaitech.edu.cn

https://doi.org/10.1016/j.isci.2019.07.036

homeostasis and redox balance, critical for primary cell transformation and lung cancer formation, but not normal mouse development.

RESULTS

Chromosome 7p Amplification and Associated Prognosis in Human Lung Adenocarcinoma (LUAD)

Genetic alterations including point mutations and copy number variations in somatic cells are the driving forces for human cancer. Recent cancer genomics efforts, such as The Cancer Genome Atlas (TCGA), enable us to systematically study the genetic alterations in cancer, and many novel oncogenes or tumor suppressors have been identified in this way (Kandoth et al., 2013; Zack et al., 2013). Here we focused on the copy number alterations of human LUAD, and observed that the short arm of chromosome 7 (7p) is among the top amplified chromosome fragments based on several independent studies (Balsara and Testa, 2002; Lu et al., 2011; Ni et al., 2013; Weir et al., 2007; Wu et al., 2015) (Figure S1A). Specifically, 53% of LUAD has amplified 7p (Table S1). In total 389 genes are located in human chromosome 7p region. In addition to LUAD, chromosome 7p is also amplified in other types of human cancers, including colon cancer, glioblastoma, prostate cancer, etc. (Table S1).

To investigate whether 7p amplification has an impact on the prognosis of patients with LUAD, we compared the survival curves of patients with LUAD with and without chromosome 7p amplification and observed that patients with LUAD with chromosome 7p amplification were significantly associated with poor prognosis compared with patients without 7p amplification (Figure S1B). In early-stage (TNM stage I) LUAD, the effect of 7p amplification on the prognosis is statistically significant, whereas in the late stages (TNM stage III and IV), 7p amplification is not significantly associated with poor patient prognosis (Figure S1C). This implicates a specific function of 7p amplification in early-stage LUAD.

As 7p is widely amplified in human cancer, some oncogenes located in 7p may be co-amplified and their expression up-regulated consequently. To identify these potential oncogenes in 7p region, we systematically compared the mRNA expression of 389 chromosome 7p genes in normal lung and LUAD samples (Table S2). *GGCT* was among the top significantly up-regulated genes when we compare LUAD with normal lung samples. This implies that *GGCT* may be one of the target genes responsible for 7p amplification-associated cancer. *GGCT* chromosome locus 7p14.3 was reported to be amplified in lung cancer (Choi et al., 2007), and in the 7p14.3 region, GGCT is the top significantly expressed up-regulated gene, suggesting that *GGCT* could also be the target of 7p14.3 amplification in lung cancer.

Stimulation of *GGCT* Transcription by Activated Ras Signaling

GGCT gene was originally identified when we compared the differentially expressed genes between $Kras^{G12D}$-expressing and control primary mouse embryonic fibroblasts (MEFs) (Figure 1A). When Ras signaling was inhibited with MEK inhibitor trametinib (0.5 μM, 24 h), we observed that *GGCT* mRNA expression was down-regulated (Figure 1B). These observations implicate that *GGCT* mRNA expression is under the regulation of oncogenic growth signaling. We cloned human *GGCT* promoter and used it to drive the transcription of luciferase reporter gene. In the presence of trametinib (0.5 μM, 24 h), *GGCT* promoter activity is also significantly decreased (Figure 1C). To further validate the induction of GGCT by Ras signaling, we knocked down *KRAS* gene in human cancer cells and observed that *GGCT* transcription is down-regulated (Figure S2). These studies imply that oncogenic Ras signal transcriptionally regulates *GGCT* expression. When combined with the observation that *GGCT* locus is amplified in cancer, *GGCT* transcription regulation by Ras oncogenic signal further supports cancer-related function of *GGCT*.

GGCT CNV Amplification in Human Cancer

The mRNA and protein expression of *GGCT* was already known to be up-regulated in various human cancers (Amano et al., 2012; Gromov et al., 2010; Kageyama et al., 2007, 2015). We checked *GGCT* mRNA expression in various human cancers and indeed found that the mRNA of *GGCT* was up-regulated in various cancers compared with each control tissue, and in several cancer types this difference reached statistical significance (Figure 2A). Based on expression difference, GGCT can be a key gene responsible for chromosome 7p amplification in human LUAD. The copy number of *GGCT* is systematically investigated in multiple human cancer samples, including lung, prostate, and colon using the TCGA database. Results confirmed *GGCT* copy number variation (CNV) amplification in multiple human cancers including LUAD

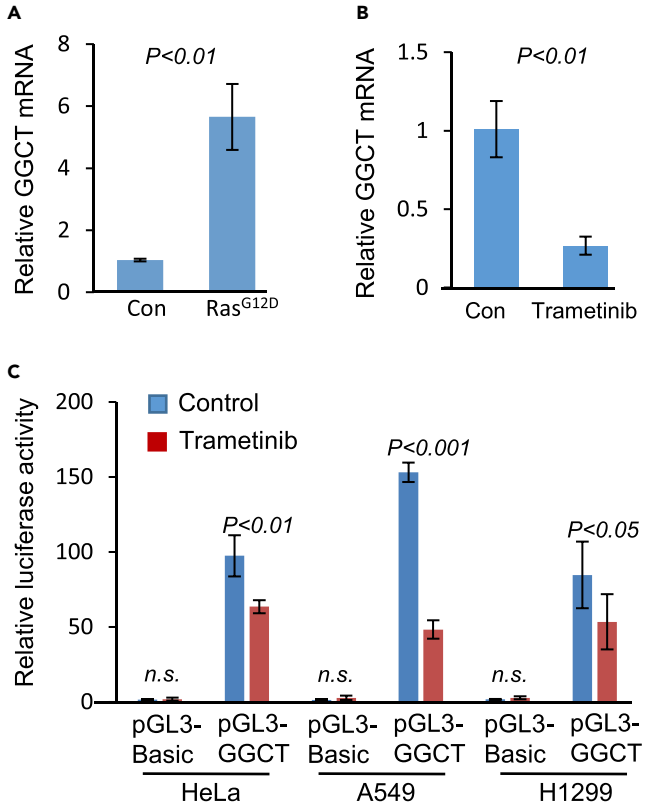

Figure 1. RAS Regulates *GGCT* Transcription

(A) Constitutively active *RAS* (*KRAS*^{G12D}) expression stimulates *GGCT* transcription in primary mouse embryonic fibroblasts (MEFs). Error bars represent mean ± SD from three experiments.

(B) Trametinib (MEK inhibitor) inhibits *GGCT* transcription in MEFs. *GGCT* mRNA was detected by real-time PCR. Error bars represent mean ± SD from three experiments.

(C) Luciferase reporter assay was performed in HeLa, A549, and H1299 cells with human *GGCT* promoter driving pGL3 vector in the presence or absence of MEK inhibitor trametinib. Significantly decreased *GGCT* promoter, but not pGL3-basic promoter, activity was observed in the presence of trametinib. Error bars represent mean ± SD of three experiments. p Values of unpaired two-tailed t test are shown.

(Figure 2B). To further evaluate the CNV status of *GGCT* in cancer, we examined *GGCT* CNV in LUAD samples by qPCR. In these LUAD samples, *GGCT* CNV is significantly up-regulated (Figure 2C).

Besides human cancer samples, *GGCT* CNV status was also systematically analyzed in human lung cancer cell lines. Results indicate that *GGCT* CNV is significantly amplified in human cancer cell lines (Figure S3A). We further evaluated *GGCT* CNV in human cancer cell lines by qPCR, the results confirming the up-regulated *GGCT* CNV in human lung cancer cell lines (Figure S3B). *GGCT* CNV and mRNA expression show significant correlation in both samples of human patients with cancer (Figure 2D) and lung cancer cell lines (Figure S3C). This implies that *GGCT* CNV amplification can directly lead to the up-regulated expression of *GGCT* mRNA. In addition, *GGCT* mRNA expression also significantly correlates with GGCT protein level in lung cancer cell lines (Figure S3D).

GGCT CNV, mRNA, and LUAD Patient Prognosis

It is known that *GGCT* mRNA and protein expression are frequently up-regulated in cancers compared with normal control tissues. However, the consequence of *GGCT* up-regulation in cancer prognosis is still not well studied. Here the prognosis of the patient with lung cancer was evaluated based on *GGCT* CNV status. Interestingly, in early-stage (TNM stage I) LUAD, patients with amplified *GGCT* CNV show significantly decreased overall survival (Figure S4A), whereas in late-stage LUAD *GGCT* CNV amplification does not lead to significantly poor prognosis (Figure S4B). This result suggests that *GGCT* CNV amplification may play a specific function in early-stage LUAD. *GGCT* mRNA expression and LUAD prognosis were also

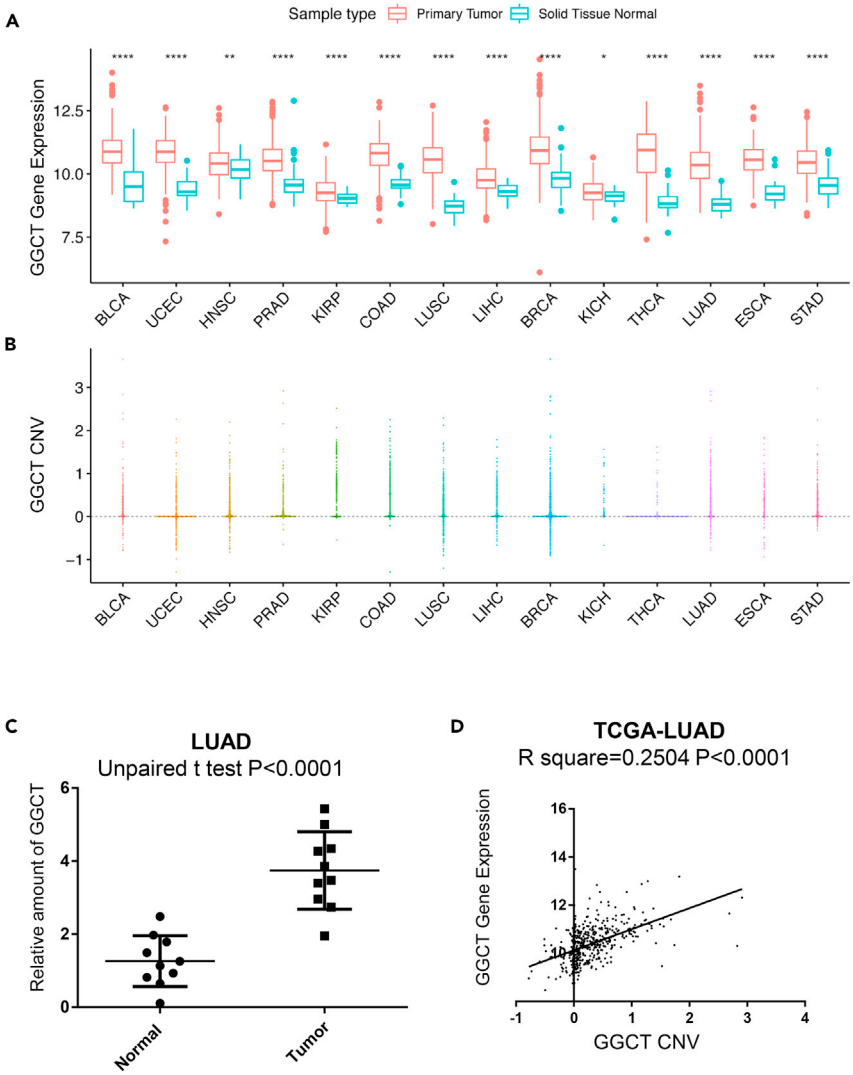

Figure 2. *GGCT* Copy Number Variation (CNV) and mRNA Expression Status in Human Cancers

(A) *GGCT* mRNA expression levels (log2 based) were statistically up-regulated (unpaired two-tailed t test) in 14 of 15 types of human cancers when compared with corresponding normal control tissues based on The Cancer Genome Atlas (TCGA) database. Only 15 of 32 TCGA cancer types have both tumor and normal control samples available, and the number of normal samples is greater than or equal to 10. ****$p < 0.0001$, **$p < 0.01$, *$p < 0.05$.

(B) *GGCT* copy number values (log2 based ratio, normal copy number is 0) obtained from GISTIC2 software in cancers as (A) are shown based on TCGA database. GISTIC2 CNV value 0 means normal copy number.

(C) *GGCT* CNV values were detected by qPCR in patients with LUAD (n = 10) and normal control (n = 10) samples. Error bars represent mean ± SD. p Values of unpaired two-tailed t test are shown.

(D) The correlation between *GGCT* CNV and mRNA in TCGA lung adenocarcinoma (LUAD) samples (n = 511).

evaluated; *GGCT* mRNA shows similar trends as *GGCT* CNV in early-stage LUAD prognosis; the difference does not reach statistical significance based on $p < 0.05$ (Figure S4C). In late-stage LUAD, the prognosis of *GGCT* mRNA does not show the same trends as in early-stage LUAD (Figure S4D). This could implicate a specific function of *GGCT* mRNA expression in cancer initiation or early-stage cancer progression. Both *GGCT* mRNA and CNV status do not show significant difference between early- and late-stage LUAD (Figures S4E and S4F). And in both stages of LUAD, GGCT mRNA and CNV have similar correlations (Figures S4G and S4H). Interestingly, *GGCT* CNV amplification or mRNA up-regulation shows similar prognosis as chromosome 7p amplification in both early- and late-stage LUAD. This further implicates the critical function of *GGCT* in cancer-associated 7p amplification.

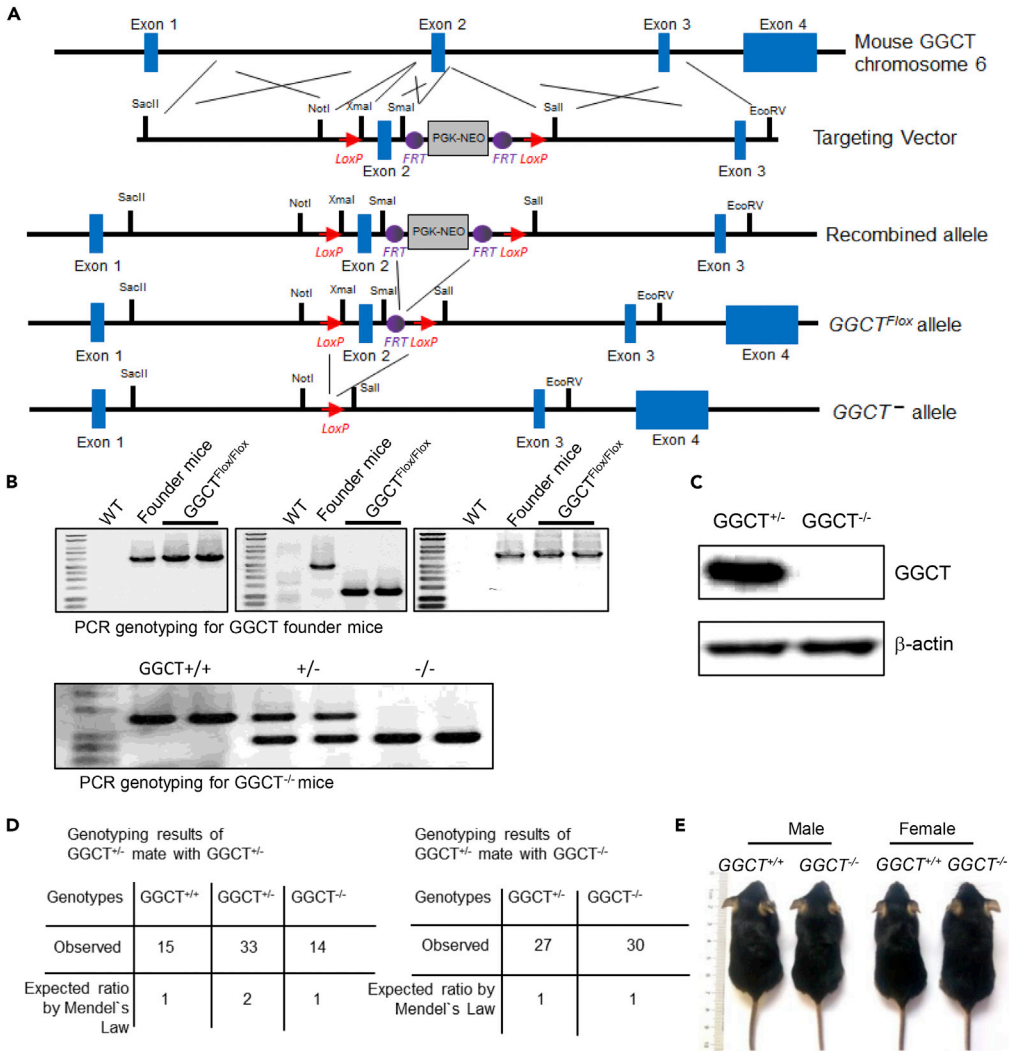

Figure 3. Generation of *GGCT* Knockout Mouse Model and *GGCT*$^{-/-}$ Mice Are Viable

(A) ES cell-targeting strategy for generating *GGCT* conditional knockout mice.

(B) PCR genotyping results for *GGCT* conditional knockout founder mice and *GGCT*$^{-/-}$ mice.

(C) Western blot analysis of *GGCT*$^{+/+}$ and *GGCT*$^{-/-}$ MEFs with anti-GGCT antibody; β-actin served as loading control.

(D) Genotyping results of *GGCT*$^{+/-}$ mouse mated with *GGCT*$^{+/-}$ mouse and *GGCT*$^{+/-}$ mouse mated with *GGCT*$^{-/-}$ mouse. In both cases, the genotype distributions of offspring are in line with Mendel's law, implicating that *GGCT* deletion is compatible with normal mouse embryonic development.

(E) Representative pictures of two-months-old male and female *GGCT*$^{+/+}$ and *GGCT*$^{-/-}$ mice.

GGCT$^{-/-}$ Mouse Generation and Analysis

No *GGCT* transgenic or knockout mouse model has ever been reported. To further investigate the function of GGCT, we generated *GGCT* conditional knockout (*GGCT*$^{Flox/Flox}$) mouse model through embryonic stem (ES) cell targeting and blastocyst injection (Figure 3A). We obtained complete *GGCT* knockout (*GGCT*$^{-/-}$) mouse by crossing *GGCT*$^{Flox/Flox}$ with EIIα-Cre mouse. The genotyping strategy is described in the Methods section, and genotyping results are shown (Figure 3B). The depletion of GGCT protein in *GGCT*$^{-/-}$ MEFs was further confirmed by western blot analysis with anti-GGCT antibody (Figure 3C). *GGCT*$^{+/-}$ mice are viable and show no apparent phenotypes. When *GGCT*$^{+/-}$ mice are crossed with *GGCT*$^{-/-}$ or *GGCT*$^{+/-}$ mice, the genotype of the pups show Mendialian distribution (Figure 3D). Adult *GGCT*$^{-/-}$ mice do not show difference in body weight when compared with wild-type control mice of similar ages (Figure S5). This indicates that *GGCT* deficiency is compatible with normal mouse development (Figure 3E).

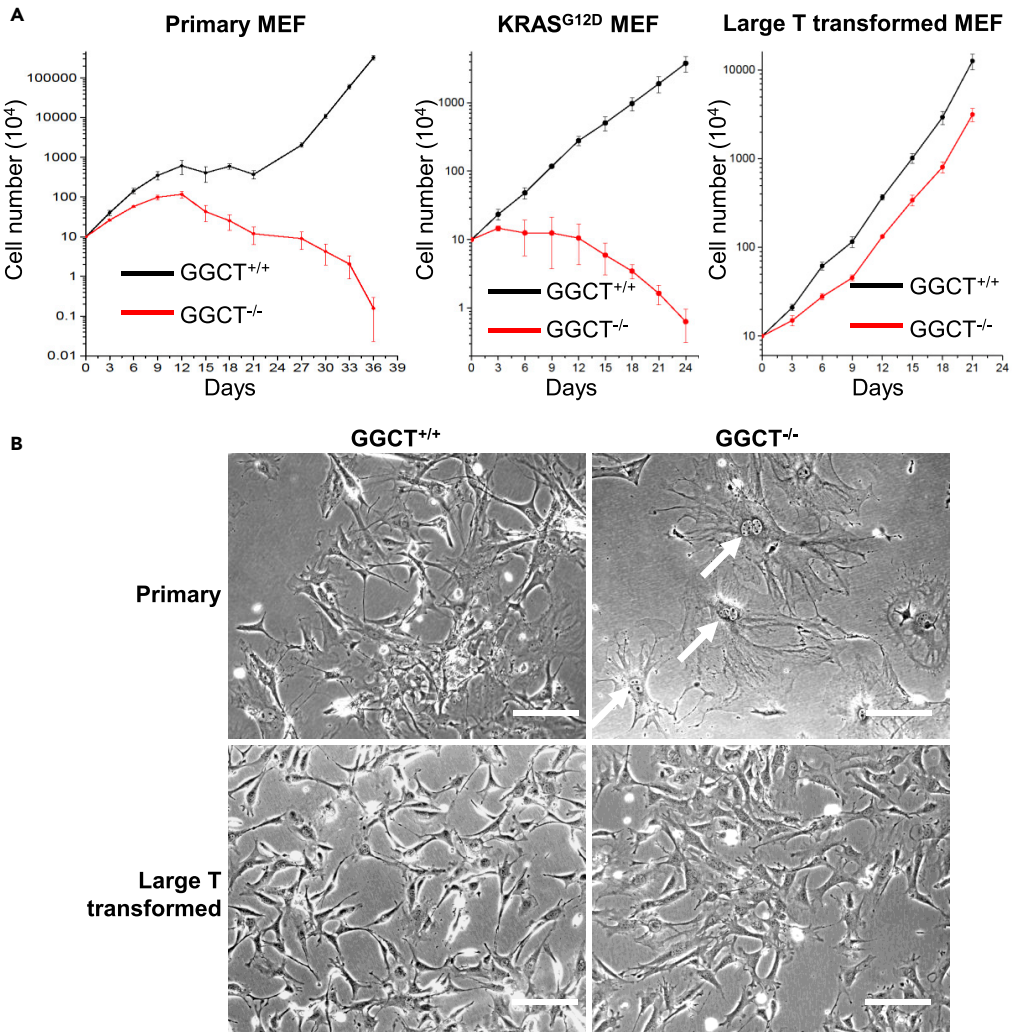

Figure 4. *GGCT*$^{-/-}$ MEFs Show Proliferation Inhibition, Senescence, and Resistance to Automatic Transformation Phenotypes

(A) Cell proliferation assay. 10 × 10^4 MEFs of indicated genotypes are seeded into 3.5-cm tissue culture dishes, and the cell numbers are counted every 3 days. Error bars represent mean ± SD of three experiments.

(B) Phase contrast images of primary and large T-transformed wild-type and *GGCT*$^{-/-}$ MEFs. Nearly all late-passage (P7) *GGCT*$^{-/-}$ MEFs are senescent, whereas same-passage primary wild-type or transformed wild-type, GGCT $^{-/-}$ MEFs do not show significant senescent features. White arrows indicate typical senescent cells, which show flat morphology and double nuclei phenotypes. Scale bar, 50 mm.

GGCT Depletion Suppresses Primary MEF Transformation and Lung Cancer Formation in *Kras G12D* Mouse Model

To further investigate the function of GGCT in primary cell proliferation and transformation. We isolated and cultured *GGCT*$^{-/-}$ and sibling control *GGCT*$^{+/+}$ embryonic day 13.5 (E13.5) MEFs from pregnant *GGCT*$^{+/-}$ female mouse. Early-stage (before passage 4) *GGCT*$^{-/-}$ MEFs can proliferate albeit at slightly slower speed, whereas late-stage *GGCT*$^{-/-}$ MEFs show significantly decreased ability in proliferation and completely lose the ability to become automatically transformed during long-passage *in vitro* culture (Figure 4A). *GGCT* deletion also completely blocked the *in vitro* proliferation of *KRAS*^{G12D}-expressing MEFs (Figure 4A). *GGCT*$^{-/-}$ MEFs also show early senescence phenotype (Figure 4B). *GGCT*$^{-/-}$ MEFs can be transformed by large T antigen (Figure 4A), which inhibits both Rb and p53 pathways (Ahuja et al., 2005). In large T antigen-expressing situation, both *GGCT*$^{-/-}$ and *GGCT*$^{+/+}$ MEFs do not show apparent senescent phenotype and can proliferate at similar speed (Figure 4). This indicates that Rb and p53 tumor suppressor may be involved in the growth arrest and senescence phenotypes of *GGCT*$^{-/-}$ MEFs.

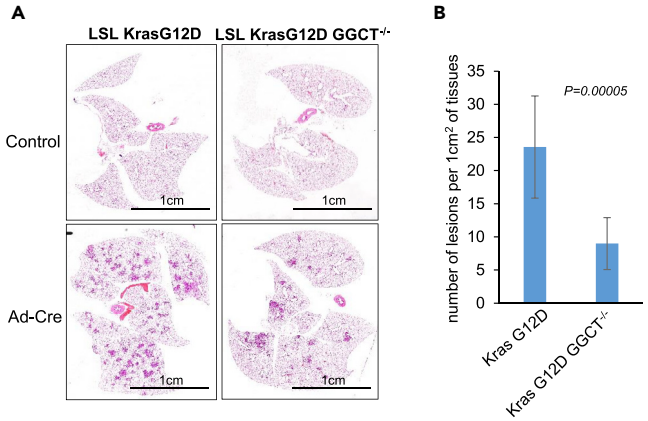

Figure 5. GGCT Is Required for Efficient Cancer Formation in Oncogenic Kras-Driven Mouse Model Lung Cancer

(A) Histology of *LSL-Kras G12D* and *GGCT*$^{-/-}$*LSL-Kras G12D* mouse lungs 12 weeks after intranasal inhalation of adenovirus Cre.

(B) Number of tumor lesions per area of lung tissue in *LSL-Kras G12D* and *GGCT*$^{-/-}$*LSL-Kras G12D* mice. Error bars represent mean ± SD of 10 animals. Unpaired two-tailed t test p value is shown. Scale bar, 1 cm.

Our study demonstrated that GGCT transcription is regulated by Ras signaling (Figure 1). To further investigate the *in vivo* function of GGCT in oncogenic Ras-induced cancer formation, we crossed *GGCT*$^{-/-}$ mouse with (Lox-Stop-Lox) *LSL- Kras G12D* mouse model and induced lung cancer formation through intranasal inhalation of Cre recombinase-expressing adenovirus (Jackson et al., 2001). Significantly decreased tumors are formed in *GGCT*$^{-/-}$ *LSL- Kras G12D* mouse compared with *LSL- Kras G12D* mouse 3 months after adenovirus Cre treatment (Figures 5A and 5B). This observation indicates that GGCT is required for efficient lung cancer formation in oncogenic *Kras*-driving cancer.

Function of GGCT in Alleviating Oncogenic Stress Signaling

To further investigate the molecular mechanism by which GGCT regulates cell proliferation, senescence, and cancer initiation, RNA sequencing (RNA-seq) analysis was performed with primary, *Kras*^{G12D}-expressing, or large T antigen-transformed *GGCT*$^{-/-}$ and GGCT$^{+/+}$ MEFs. The RNA-seq data generated in this study has been deposited in NCBI SRA database with the accession number SRA: PRJNA554607. In both primary and *Kras*^{G12D}-expressing situations, cell cycle gene signature, specifically Rb-E2F gene signature, is the top different gene signature when comparing *GGCT*$^{-/-}$ and GGCT$^{+/+}$ MEFs (Table S3 and Figure S6), whereas in large T antigen-transformed situation, this Rb-E2F signature does not appear (Table S3), and this observation is in line with the fact that large T antigen is able to block Rb tumor suppressor pathway.

GGCT deficiency has no apparent effect on mouse embryonic development and tissue function (Figure 3). In contrast, during *Kras*^{G12D} oncogenic transformation processes, the accumulated cellular stresses need the presence of GGCT to become adapted, and consequently loss of *GGCT* significantly impaired cell proliferation in these situations (Figure 4). Cellular stress represented by reactive oxygen species (ROS) is known to be accumulated during oncogene transformation process (Behrend et al., 2003), and uncontrolled ROS stress can contribute to cell proliferation inhibition and senescence (Pelicano et al., 2004). We did observe that in *GGCT*$^{-/-}$ MEFs, ROS level is significantly up-regulated as measured by flow cytometry with ROS indicator carboxy-H2DCFDA (Figure 6A and B).

GGCT is known to have γ-glutamyl cyclotransferase enzyme activity (Oakley et al., 2008). And in plant, this enzyme activity was reported to participate in GSH homeostasis (Kumar et al., 2015; Paulose et al., 2013). However, the function of GGCT in GSH metabolism has not been reported. We then checked the GSH level in MEFs and observed that *GGCT*$^{-/-}$ MEFs have significantly decreased GSH level compared with wild-type sibling control MEFs (Figure 6C). This decreased GSH level could contribute to the elevated oxidative stress observed in *GGCT*$^{-/-}$ MEFs, because GSH is an important antioxidant in cells. Our study thus suggests that GGCT alleviates oncogenic stress by regulating GSH-ROS metabolism. The cytoplasmic-localized GGCT (Figures S7 and S8) could contribute to intracellular GSH synthesis by regulating the recycling of GSH synthesis substrates (Paulose et al., 2013). In supporting this hypothesis, we observed that in

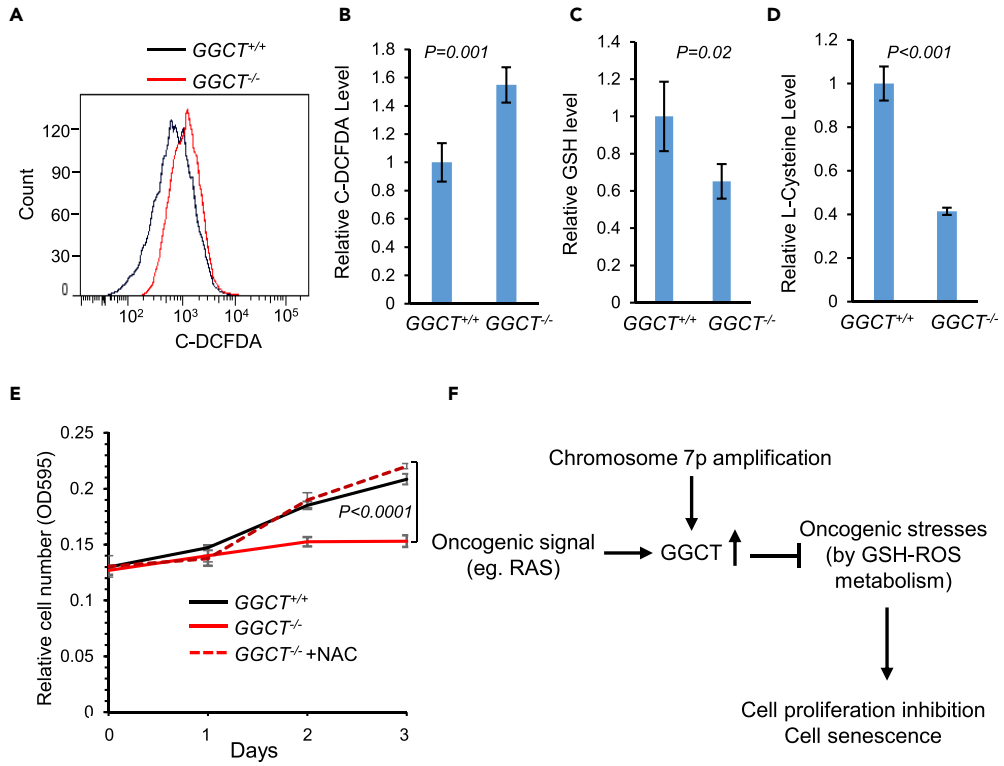

Figure 6. GGCT in Cellular Stress Alleviation

(A, B) Cellular ROS level was quantified by carboxy-H2DCFDA flow cytometry in primary wild-type and *GGCT*$^{-/-}$ MEFs; error bars represent mean ± SD of four experiments.

(C) GSH level was quantified by mass spectrometry in primary wild-type and *GGCT*$^{-/-}$ MEFs; error bars represent mean ± SD of three experiments.

(D) L-cysteine level was quantified by mass spectrometry in primary wild-type and *GGCT*$^{-/-}$ MEFs; error bars represent mean ± SD of three experiments.

(E) The proliferation defect of *GGCT*$^{-/-}$ MEFs can be rescued by ROS scavenger N-acetylcysteine (NAC, 1 mM) treatment. Error bars represent mean ± SD of three experiments.

(F) Proposed model for *GGCT* function in cancer. Both oncogenic signal (like RAS activation) and chromosomal 7p14.3 locus amplification lead to *GGCT* expression up-regulation in human cancers. GGCT helps to alleviate oncogenic stress by regulating GSH-ROS metabolism. In the absence of GGCT, the accumulated cellular stress leads to cell proliferation arrest and cell senescence. For all comparisons, p values of unpaired two-tailed t test are shown.

GGCT-deficient MEFs, intracellular L-cysteine level is significantly decreased compared with wild-type control MEFs (Figure 6D). Furthermore, the proliferation defect of *GGCT*$^{-/-}$ MEFs can be rescued by ROS scavenger N-acetylcysteine (NAC) treatment (Figure 6E), suggesting that GGCT-regulated GSH-ROS pathway is required for primary cell *in vitro* proliferation. In summary, our comprehensive cancer genomic and mouse model studies indicate that both oncogenic signal (Ras activation) and chromosomal 7p amplification lead to *GGCT* expression up-regulation in human cancers. GGCT can help to alleviate cellular stress by regulating GSH-ROS metabolism. In the absence of GGCT, the accumulated cellular stress leads to Rb activation, and consequently cell proliferation arrest and cell senescence (Figure 6F).

DISCUSSION

Oncogenic transformation in somatic cells is accompanied by various types of cellular stresses (Solimini et al., 2007). Inability to handle these cellular stresses will lead to cellular senescence (Braig and Schmitt, 2006; Kuilman et al., 2010). Oncogenic stress could also be exploited to selectively kill cancer cells but not normal somatic cells through stress sensitization or stress overload (Luo et al., 2009). However, how to alleviate these oncogenic transformation-associated cellular stresses is still a key question for cancer research. Here we report that GGCT functions downstream of common oncogenic signal (like Ras) and is required for the alleviation of ROS stress during oncogenic transformation. GGCT could modulate ROS balance by regulating GSH synthesis.

GSH is synthesized in the cytoplasm, and the availability of L-cysteine is the key determinant of GSH biosynthesis (Lu, 2013). Before the identification of ChaC1 as the first cytosolic pathway for GSH degradation in mammalian cells (Kumar et al., 2012), GSH was thought to be degraded exclusively in the extracellular space by membrane-bound GGT to cysteinylglycine and γ-glutamyl-amino acid dipeptide (Ballatori et al., 2009). One of the best acceptor amino acids for GGT enzymatic reaction is L-cystine (Thompson and Meister, 1976). In the absence of GGT, intracellular GSH level is down-regulated due to decreased availability of intracellular L-cysteine (Bachhawat and Kaur, 2017; Hanigan, 2014). Based on our experimental data, *GGCT* deficiency also leads to decreased intracellular L-cysteine and consequently GSH down-regulation. Thus membrane-bound GGT and cytoplasmic GGCT could be functionally related in GSH homeostasis by recycling L-cysteine. In supporting this interesting hypothesis, GGT expression was also observed to be up-regulated in various human cancers (Hanigan, 2014).

It has already been reported that GGCT protein or mRNA expression is up-regulated in various cancers, including bladder urothelial carcinoma (Kageyama et al., 2007), breast cancer (Gromov et al., 2010), and osteosarcoma (Uejima et al., 2011). GGCT has also been proposed as a biomarker for cancer (Kageyama et al., 2015). However, it was still not known if GGCT up-regulation is a simple consequence of cancer progression, or GGCT is selected to be up-regulated during cancer initiation and progression, and thus can have cancer-driving ability. Bona fide cancer-driving oncogenes are often selected to be amplified through genetic alterations. Here we provide comprehensive and systematic cancer genomics analysis of *GGCT* gene. Our analysis was based on TCGA, and the results have been verified by performing experiments in human cancer samples or cancer cell lines. We found significant *GGCT* genetic amplification in human LUAD and other cancers, importantly *GGCT*, maybe the target gene for chromosome 7p or 7p14.3 amplification in cancer. The amplification of *GGCT* CNV in LUAD compared with normal lung tissue suggests a selection pressure on *GGCT* amplification during LUAD initiation or progression. CNV amplification directly leads to *GGCT* mRNA and protein up-regulation, implicating a potential oncogenic role of GGCT in LUAD.

In early-stage LUAD, *GGCT* CNV up-regulation is associated with significantly decreased patient prognosis, whereas in late stage of LUAD, the prognosis of patients with *GGCT* CNV amplification is not significantly decreased compared with patients without *GGCT* CNV amplification. Similarly, the prognosis of *GGCT* mRNA expression shows similar trends as *GGCT* CNV. In early-stage cancer, GGCT up-regulation makes a difference in patient prognosis, meaning a specific function of GGCT in early-stage cancer, probably in cancer initiation. Our *in vitro* cell culture experiments support the critical function of GGCT in primary cell transformation. And these data are in line with the cancer genomic analysis data, because somatic cell tumorigenic transformation is usually the initial step in cancer progression.

Here we also reported the generation of the first *GGCT* knockout mouse model. *GGCT* deficiency is compatible with normal mouse development and tissue function, but it is required for primary MEFs' *in vitro* growth and transformation. *GGCT* is transcriptionally regulated by oncogenic Ras signal, and in oncogenic Ras-expressing MEFs, *GGCT* loss strongly blocked cell proliferation. More importantly, using a *LSL-Kras G12D* lung cancer mouse model, we demonstrated a critical role of *GGCT* in oncogenic Ras-induced *in vivo* tumorigenesis. These data suggested that GGCT could be targeted to specifically block cancer cell growth, and at the same time to not interrupt normal tissue function.

In summary, here we provide human cancer genomic evidence supporting the oncogenic function of GGCT. We identify GGCT as a downstream target of oncogenic Ras signaling, and that it functions as oncogenic stress alleviator by regulating GSH-ROS metabolism. $GGCT^{-/-}$ mouse show normal development; however, *GGCT* deficiency inhibits cancer cell proliferation and primary cell transformation and reduces lung cancer formation in *Kras G12D* mouse model. These observations and mechanism study suggest that the selectively amplified *GGCT* in cancer cells can be a therapeutic target for cancer treatment. Furthermore, the newly identified GSH regulator will have implications for understanding GSH homeostasis and oncogenic stress alleviation.

Limitations of the Study

There are several limitations for this study. First, the detailed mechanism by which GGCT regulates GSH synthesis is not clear. The role of γ-glutamyl cyclotransferase enzyme activity in this function is also not clear. In addition, the molecular link between GSH-ROS metabolism and cell transformation is still unknown, and this requires further study.

METHODS

All methods can be found in the accompanying Transparent Methods supplemental file.

DATA AND CODE AVAILABILITY

The accession number for the RNA-seq data reported in this paper is SRA: PRJNA554607.

SUPPLEMENTAL INFORMATION

Supplemental Information can be found online at https://doi.org/10.1016/j.isci.2019.07.036.

ACKNOWLEDGMENTS

We thank ShanghaiTech Mass-spectrometry core facility member Piliang Hao and Zhaomei Shi for help in GSH and L-cysteine quantification analysis. We thank Hongbin Ji of Chinese Academy of Sciences for providing *LSL-Kras G12D* mouse for mating. We thank Raymond Shuter for editing the text. We thank ShanghaiTech University High Performance Computing Public Service Platform for computing services. This work was supported in part by the Shanghai Pujiang Program (16PJ1407400), the National Natural Science Foundation of China (31771373), and startup funding from ShanghaiTech University.

AUTHOR CONTRIBUTIONS

S.W. performed *GGCT* cancer genomic analysis; Z.H., J.Z., and X.-S.L. performed MEFs related experiments; Y.S. performed mouse mating, genotyping, MEF preparation, and *GGCT* transcriptional regulation experiments; Z.H., S.W., F.Z., and X.-S.L. participated in study design, discussion, and manuscript preparation; X.W. performed GGCT immunofluorescence staining and participated in ES cell screening for *GGCT* knockout mouse; J.H. participated in mass spectrometry experiments and project discussion. Y.C. participated in project discussion; X.-S.L. supervised the study and wrote the manuscript.

DECLARATION OF INTERESTS

The authors declare no potential conflicts of interest.

Received: November 4, 2018
Revised: January 30, 2019
Accepted: July 23, 2019
Published: September 27, 2019

REFERENCES

Ahuja, D., Saenz-Robles, M.T., and Pipas, J.M. (2005). SV40 large T antigen targets multiple cellular pathways to elicit cellular transformation. Oncogene *24*, 7729–7745.

Amano, T., Eishi, Y., Yamada, T., Uchida, K., Minegishi, K., Tamura, T., Kobayashi, D., Hiroshi, K., Suzuki, T., and Board, P.G. (2012). Widespread expression of gamma-glutamyl cyclotransferase suggests it is not a general tumor marker. J. Histochem. Cytochem. *60*, 76–86.

Anderson, M.E. (1998). Glutathione: an overview of biosynthesis and modulation. Chem. Biol. Interact. *111-112*, 1–14.

Bachhawat, A.K., and Kaur, A. (2017). Glutathione degradation. Antioxid. Redox Signal. *27*, 1200–1216.

Ballatori, N., Krance, S.M., Notenboom, S., Shi, S., Tieu, K., and Hammond, C.L. (2009). Glutathione dysregulation and the etiology and progression of human diseases. Biol. Chem. *390*, 191–214.

Balsara, B.R., and Testa, J.R. (2002). Chromosomal imbalances in human lung cancer. Oncogene *21*, 6877–6883.

Behrend, L., Henderson, G., and Zwacka, R.M. (2003). Reactive oxygen species in oncogenic transformation. Biochem. Soc. Trans. *31*, 1441–1444.

Braig, M., and Schmitt, C.A. (2006). Oncogene-induced senescence: putting the brakes on tumor development. Cancer Res. *66*, 2881–2884.

Chi, Z., Byrne, S.T., Dolinko, A., Harraz, M.M., Kim, M.S., Umanah, G., Zhong, J., Chen, R., Zhang, J., Xu, J., et al. (2014). Botch is a gamma-glutamyl cyclotransferase that deglycinates and antagonizes Notch. Cell Rep. *7*, 681–688.

Choi, Y.W., Choi, J.S., Zheng, L.T., Lim, Y.J., Yoon, H.K., Kim, Y.H., Wang, Y.P., and Lim, Y. (2007). Comparative genomic hybridization array analysis and real time PCR reveals genomic alterations in squamous cell carcinomas of the lung. Lung Cancer *55*, 43–51.

Cox, A.D., Fesik, S.W., Kimmelman, A.C., Luo, J., and Der, C.J. (2014). Drugging the undruggable RAS: mission possible? Nat. Rev. Drug Discov. *13*, 828–851.

Gromov, P., Gromova, I., Friis, E., Timmermans-Wielenga, V., Rank, F., Simon, R., Sauter, G., and Moreira, J.M. (2010). Proteomic profiling of mammary carcinomas identifies C7orf24, a gamma-glutamyl cyclotransferase, as a potential cancer biomarker. J. Proteome Res. *9*, 3941–3953.

Hanigan, M.H. (2014). Gamma-glutamyl transpeptidase: redox regulation and drug resistance. Adv. Cancer Res. *122*, 103–141.

Jackson, E.L., Willis, N., Mercer, K., Bronson, R.T., Crowley, D., Montoya, R., Jacks, T., and Tuveson, D.A. (2001). Analysis of lung tumor initiation and progression using conditional expression of oncogenic K-ras. Genes Dev. *15*, 3243–3248.

Kageyama, S., Hanada, E., Ii, H., Tomita, K., Yoshiki, T., and Kawauchi, A. (2015). Gamma-glutamylcyclotransferase: a novel target molecule for cancer diagnosis and treatment. Biomed. Res. Int. *2015*, 345219.

Kageyama, S., Iwaki, H., Inoue, H., Isono, T., Yuasa, T., Nogawa, M., Maekawa, T., Ueda, M., Kajita, Y., Ogawa, O., et al. (2007). A novel tumor-related protein, C7orf24, identified by proteome

differential display of bladder urothelial carcinoma. Proteomics Clin. Appl. *1*, 192–199.

Kandoth, C., McLellan, M.D., Vandin, F., Ye, K., Niu, B., Lu, C., Xie, M., Zhang, Q., McMichael, J.F., Wyczalkowski, M.A., et al. (2013). Mutational landscape and significance across 12 major cancer types. Nature *502*, 333–339.

Kuilman, T., Michaloglou, C., Mooi, W.J., and Peeper, D.S. (2010). The essence of senescence. Genes Dev. *24*, 2463–2479.

Kumar, A., Tikoo, S., Maity, S., Sengupta, S., Sengupta, S., Kaur, A., and Bachhawat, A.K. (2012). Mammalian proapoptotic factor ChaC1 and its homologues function as gamma-glutamyl cyclotransferases acting specifically on glutathione. EMBO Rep. *13*, 1095–1101.

Kumar, S., Kaur, A., Chattopadhyay, B., and Bachhawat, A.K. (2015). Defining the cytosolic pathway of glutathione degradation in Arabidopsis thaliana: role of the ChaC/GCG family of gamma-glutamyl cyclotransferases as glutathione-degrading enzymes and AtLAP1 as the Cys-Gly peptidase. Biochem. J. *468*, 73–85.

Lu, S.C. (2013). Glutathione synthesis. Biochim. Biophys. Acta *1830*, 3143–3153.

Lu, T.P., Lai, L.C., Tsai, M.H., Chen, P.C., Hsu, C.P., Lee, J.M., Hsiao, C.K., and Chuang, E.Y. (2011). Integrated analyses of copy number variations and gene expression in lung adenocarcinoma. PLoS One *6*, e24829.

Luo, J., Solimini, N.L., and Elledge, S.J. (2009). Principles of cancer therapy: oncogene and non-oncogene addiction. Cell *136*, 823–837.

Meister, A. (1974). Glutathione, metabolism and function via the gamma-glutamyl cycle. Life Sci. *15*, 177–190.

Meister, A. (1988). Glutathione metabolism and its selective modification. J. Biol. Chem. *263*, 17205–17208.

Ni, X., Zhuo, M., Su, Z., Duan, J., Gao, Y., Wang, Z., Zong, C., Bai, H., Chapman, A.R., Zhao, J., et al. (2013). Reproducible copy number variation patterns among single circulating tumor cells of lung cancer patients. Proc. Natl. Acad. Sci. U S A *110*, 21083–21088.

Oakley, A.J., Yamada, T., Liu, D., Coggan, M., Clark, A.G., and Board, P.G. (2008). The identification and structural characterization of C7orf24 as gamma-glutamyl cyclotransferase. An essential enzyme in the gamma-glutamyl cycle. J. Biol. Chem. *283*, 22031–22042.

Paulose, B., Chhikara, S., Coomey, J., Jung, H.I., Vatamaniuk, O., and Dhankher, O.P. (2013). A gamma-glutamyl cyclotransferase protects Arabidopsis plants from heavy metal toxicity by recycling glutamate to maintain glutathione homeostasis. Plant Cell *25*, 4580–4595.

Pelicano, H., Carney, D., and Huang, P. (2004). ROS stress in cancer cells and therapeutic implications. Drug Resist. Updat. *7*, 97–110.

Solimini, N.L., Luo, J., and Elledge, S.J. (2007). Non-oncogene addiction and the stress phenotype of cancer cells. Cell *130*, 986–988.

Thompson, G.A., and Meister, A. (1976). Hydrolysis and transfer reactions catalyzed by gamma-glutamyl transpeptidase; evidence for separate substrate sites and for high affinity of L-cystine. Biochem. Biophys. Res. Commun. *71*, 32–36.

Uejima, D., Nishijo, K., Kajita, Y., Ishibe, T., Aoyama, T., Kageyama, S., Iwaki, H., Nakamura, T., Iida, H., Yoshiki, T., et al. (2011). Involvement of cancer biomarker C7orf24 in the growth of human osteosarcoma. Anticancer Res. *31*, 1297–1305.

Weir, B.A., Woo, M.S., Getz, G., Perner, S., Ding, L., Beroukhim, R., Lin, W.M., Province, M.A., Kraja, A., Johnson, L.A., et al. (2007). Characterizing the cancer genome in lung adenocarcinoma. Nature *450*, 893–898.

Wu, K., Zhang, X., Li, F., Xiao, D., Hou, Y., Zhu, S., Liu, D., Ye, X., Ye, M., Yang, J., et al. (2015). Frequent alterations in cytoskeleton remodelling genes in primary and metastatic lung adenocarcinomas. Nat. Commun. *6*, 10131.

Zack, T.I., Schumacher, S.E., Carter, S.L., Cherniack, A.D., Saksena, G., Tabak, B., Lawrence, M.S., Zhsng, C.Z., Wala, J., Mermel, C.H., et al. (2013). Pan-cancer patterns of somatic copy number alteration. Nat. Genet. *45*, 1134–1140.

ISCI, Volume *19*

Supplemental Information

Ras Downstream Effector GGCT

Alleviates Oncogenic Stress

Zaoke He, Shixiang Wang, Yuanyuan Shao, Jing Zhang, Xiaolin Wu, Yuxing Chen, Junhao Hu, Feng Zhang, and Xue-Song Liu

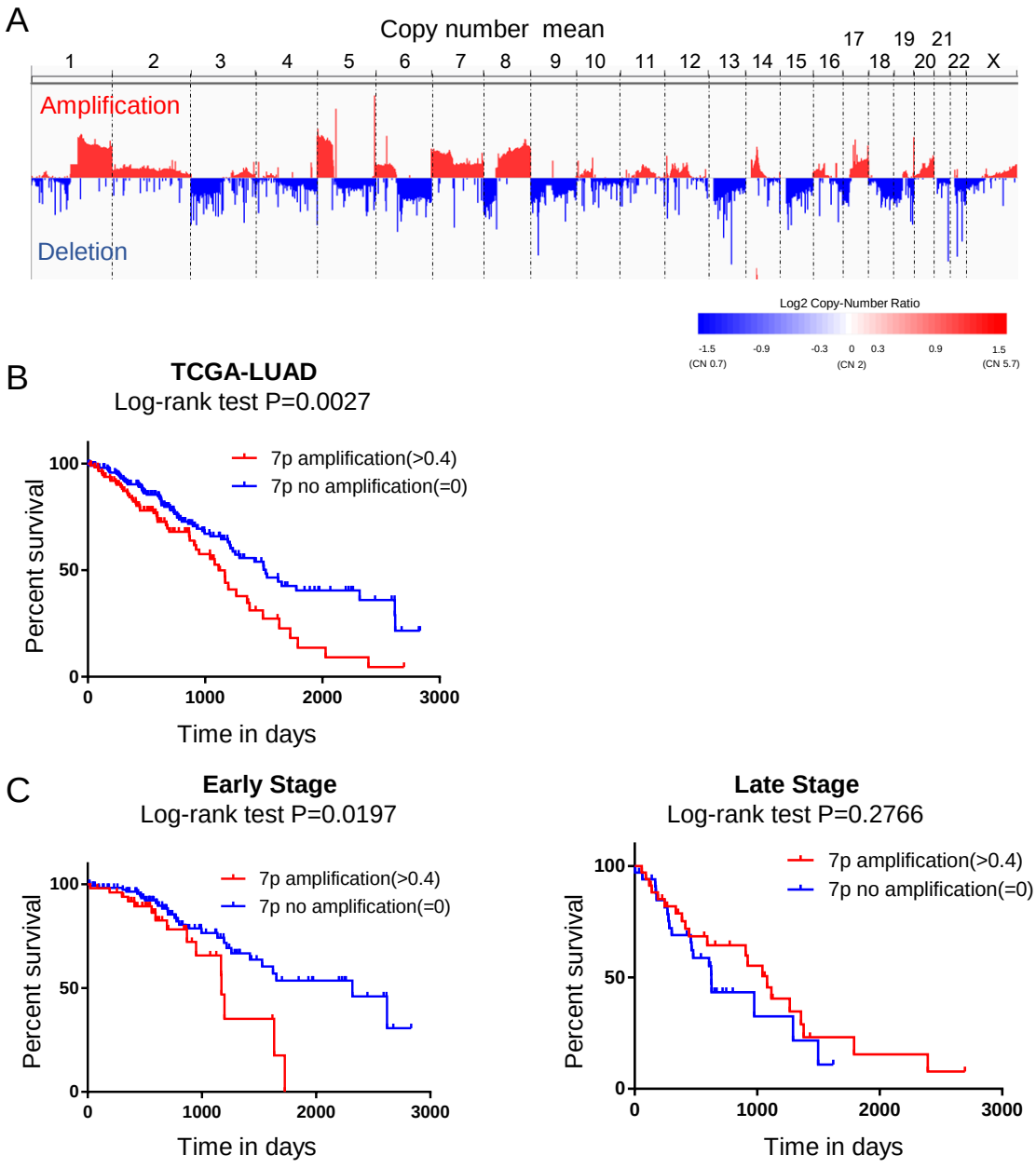

Figure S1. Chromosome 7p amplification and associated patient prognosis in human lung adenocarcinoma (LUAD), Related to Figure 2. (A) Chromosomal level copy number variation status of human LUAD based on TCGA databases.

(B) Kaplan–Meier overall survival curve of LUAD patients with (n=116) or without (n=199) Chromosome 7p amplification are shown. 7p amplification is significantly associated with poor overall survival of LUAD patients.

(C) Kaplan–Meier overall survival curve of early stage (left panel) LUAD patients with (n=51) or without (n=117) chromosome 7p amplification, and also Kaplan–Meier overall survival curves of late stage (right panel) LUAD patients with (n=35) or without (n=34) 7p amplification are shown.

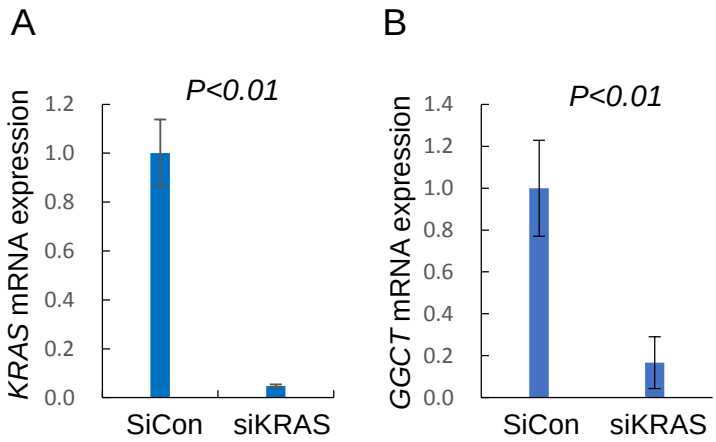

Figure S2. KRAS knockdown leads to decreased GGCT transcription in cancer cells, Related to Figure 1.

KRAS gene was knockdown in A549 lung cancer cells with siRNA. The mRNA expression of *KRAS* (A) and *GGCT* (B) were quantified with qPCR. Error bars represent mean ± s.d. from three experiments.

Chromosome 7p copy number variation

cancer type	Arm	# Genes	Amp frequency	Amp z-score	Amp q-value	Del Frequency	Del z-score	Del q-value
COADREAD	7p	389	0.57	25.2	0	0.02	-6.83	1
COAD	7p	389	0.55	16.3	0	0.02	-7.05	1
GBMLGG	7p	389	0.55	49.1	0	0.02	-5.66	1
GBM	7p	389	0.82	54.1	0	0.07	-1.25	1
KIPAN	7p	389	0.42	24.6	0	0.01	-8.45	1
KIRC	7p	389	0.32	14.7	0	0.01	-6.24	1
KIRP	7p	389	0.6	23.5	0	0.01	-3.91	1
LGG	7p	389	0.23	13.2	0	0.01	-4.83	1
LUAD	7p	389	0.53	9.08	0	0.19	-4.86	1
PRAD	7p	389	0.21	14	0	0	-4.73	1
READ	7p	389	0.62	12.4	0	0.05	-3.35	1
SKCM	7p	389	0.58	12.9	0	0.13	-4.21	1
STAD	7p	389	0.46	10.3	0	0.11	-4.82	1
STES	7p	389	0.5	11.8	0	0.14	-5.68	1
TGCT	7p	389	0.82	11.6	0	0.07	-3.26	1
HNSC	7p	389	0.36	6.01	6.47E-09	0.11	-5.95	1
ESCA	7p	389	0.63	6.06	6.76E-09	0.26	-2.55	1
LUSC	7p	389	0.53	5.72	3.20E-08	0.26	-4.51	1
LIHC	7p	389	0.3	5.06	9.33E-07	0.08	-4.77	1
BLCA	7p	389	0.43	4.9	2.80E-06	0.12	-6.58	1
ACC	7p	389	0.56	4.52	1.06E-05	0.14	-2.63	0.999
DLBC	7p	389	0.33	4.67	3.02E-05	0.06	-0.91	0.984
THCA	7p	389	0.04	4.51	3.26E-05	0	-2.53	0.995
PAAD	7p	389	0.28	4.56	3.47E-05	0.03	-4.07	1
PCPG	7p	389	0.17	4.7	5.38E-05	0.01	-2.9	1
BRCA	7p	389	0.31	3.84	0.000424	0.16	-5.76	1
THYM	7p	389	0.12	3.93	0.000587	0.03	-0.991	0.981
MESO	7p	389	0.29	3.44	0.012	0	-3.36	1
UVM	7p	389	0.11	2.44	0.0275	0	-1.97	0.985
SARC	7p	389	0.35	2.18	0.164	0.2	-2.53	1
KICH	7p	389	0.37	2.19	0.292	0.02	-3.4	1
UCEC	7p	389	0.13	0.265	0.853	0.1	-1.56	1
LAML	7p	389	0.01	-0.907	0.951	0.09	8.96	0
CHOL	7p	389	0.22	-0.0205	0.989	0.14	-1.07	0.982
CESC	7p	389	0.14	-2.82	1	0.1	-4.08	1
OV	7p	389	0.38	-0.625	1	0.32	-3.1	1
UCS	7p	389	0.45	-0.285	1	0.42	-0.635	0.975

Table S1. **Chromosome 7p amplification in various cancer, Related to Figure 2.**

Chromosome 7p copy number variation status in different types of human cancer are shown. For both amplification and deletion, the table has columns for the frequency of amplification (or deletion) of the arm, and associated Z score and Q value.

7p 386 gene

Gene Symbol	logFC >0	AveExpr	t	P.Value	adj.P.Val	B	Locus ID	Cytoband
BZW2	1.409732	6.245525	12.87138	1.16E-26	5.36E-25	49.70866	28969	7p21.1
EIF2AK1	0.972654	7.641871	12.25481	6.16E-25	2.32E-23	45.71858	27102	7p22.1
KDELR2	1.02023	8.261081	11.05695	1.35E-21	3.46E-20	38.06302	11014	7p22.1
CBX3	1.053988	7.407541	10.7314	1.08E-20	2.45E-19	35.98831	11335	7p15.2
DDX56	0.844272	5.975058	9.914304	1.88E-18	3.21E-17	30.88133	54606	7p13
GGCT	1.413713	5.456169	9.896164	2.1E-18	3.57E-17	30.84137	79017	7p14.3
TBRG4	1.046129	5.548764	9.884706	2.26E-18	3.82E-17	30.73586	9238	7p13
ANLN	3.486002	4.231763	9.805604	3.71E-18	6.12E-17	30.54145	54443	7p14.2
PSMG3	1.449531	4.773457	9.350314	6.26E-17	8.8E-16	27.55179	84262	7p22.3
AIMP2	1.113548	4.447288	9.110528	2.73E-16	3.49E-15	26.1025	7965	7p22.1
GARS	0.984559	6.704351	9.034754	4.35E-16	5.41E-15	25.45433	2617	7p14.3
CCT6A	0.977182	7.425921	8.874154	1.16E-15	1.35E-14	24.47984	908	7p11.2
TTYH3	1.483671	6.624684	8.849724	1.34E-15	1.55E-14	24.3525	80727	7p22.3

7p14.3 45 gene

Gene Symbol	logFC >0	AveExpr	t	P.Value	adj.P.Val	B	Locus ID	Cytoband
GGCT	1.413713	5.456169	9.896164	2.1E-18	3.57E-17	30.84137	79017	7p14.3
GARS	0.984559	6.704351	9.034754	4.35E-16	5.41E-15	25.45433	2617	7p14.3
AVL9	1.156238	4.318109	7.928283	3.22E-13	2.64E-12	19.12399	23080	7p14.3
LSM5	0.790194	4.903927	7.057501	4.52E-11	2.79E-10	14.14556	23658	7p14.3
PLEKHA8	0.950119	2.489666	6.933485	8.93E-11	5.32E-10	13.78726	84725	7p14.3
DPY19L1	1.004306	6.383713	6.431107	1.32E-09	6.66E-09	10.71815	23333	7p14.3
NPSR1	2.615909	-4.82135	5.397301	2.33E-07	8.52E-07	6.698606	387129	7p14.3
ZNRF2	0.501314	4.763988	4.926464	2.03E-06	6.43E-06	3.66741	223082	7p14.3
FKBP14	0.43418	3.573499	3.945982	0.000118	0.000281	-0.0602	55033	7p14.3
SCRN1	0.495392	6.361466	3.091289	0.002342	0.004468	-3.09808	9805	7p14.3
CCDC129	1.572301	-2.09954	2.368098	0.019043	0.030643	-3.97082	223075	7p14.3
RP9	0.217461	3.119666	2.03776	0.043178	0.064404	-5.41377	6100	7p14.3
WIPF3	0.575624	-0.92826	1.832223	0.068729	0.098161	-5.24634	644150	7p14.3

Table S2. Chromosome 7p and 7p14.3 gene expression in LUAD, Related to Figure 2.

mRNA expression of chromosome 7p (386 gene) and 7p14.3 (45 gene) genes are ranked based on the statistical difference between normal control and LUAD based on TCGA RNA-seq data.

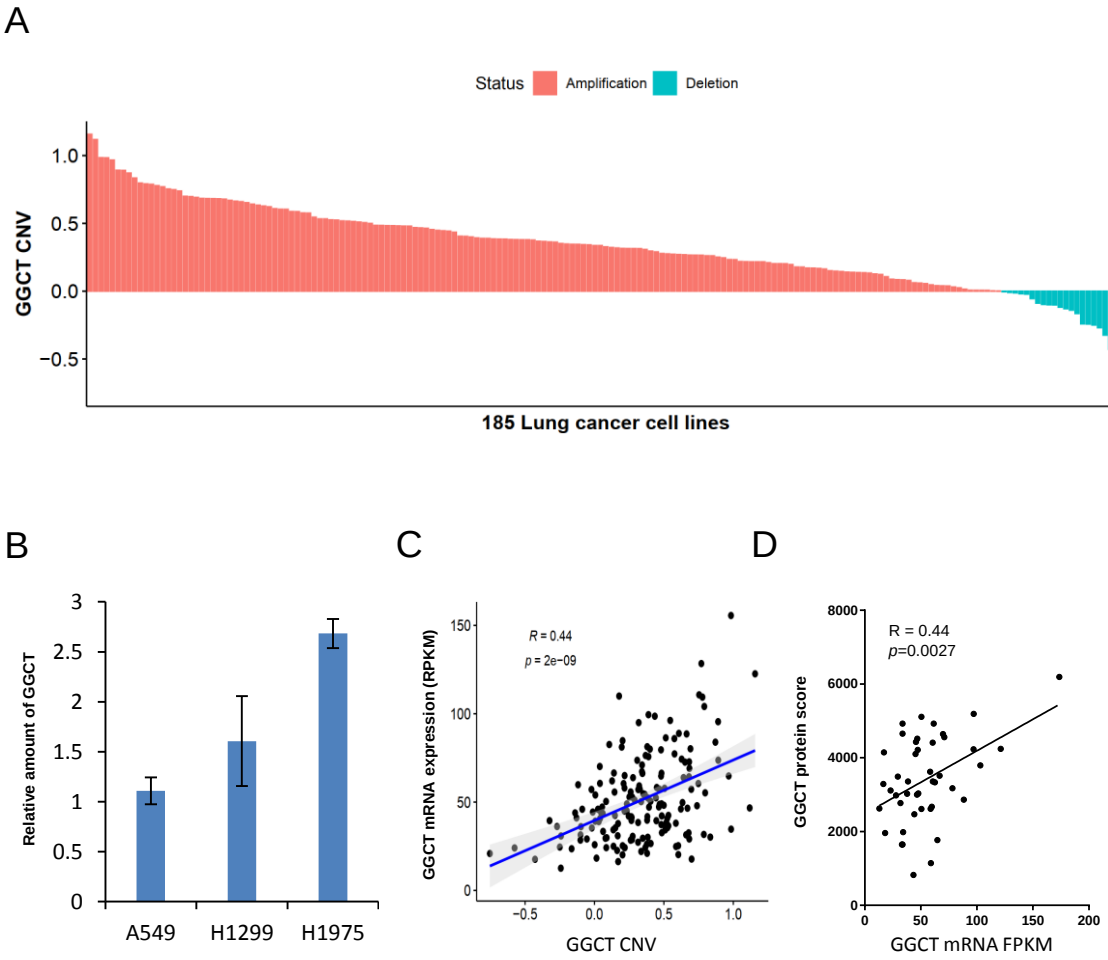

Figure S3. *GGCT* CNV amplification in human lung cancer cell lines, Related to Figure 2.

(A) *GGCT* GISTIC2 CNV values in 185 lung cancer cell lines was shown based on Cancer Cell Line Encyclopedia (CCLE) database. Majority of lung cancer cell lines displayed amplification of *GGCT* locus.

(B) *GGCT* CNV values were quantified by qPCR in three lung cancer cell lines (A549, H1299 and H1975). Error bars represent mean ± s.d. of three experiments.

(C) Correlation between *GGCT* CNV and mRNA expression in lung cancer cell lines (n=172).

(D) Correlation between *GGCT* mRNA and protein expression in lung cancer cell lines (n=44) based on data from the human protein atlas.

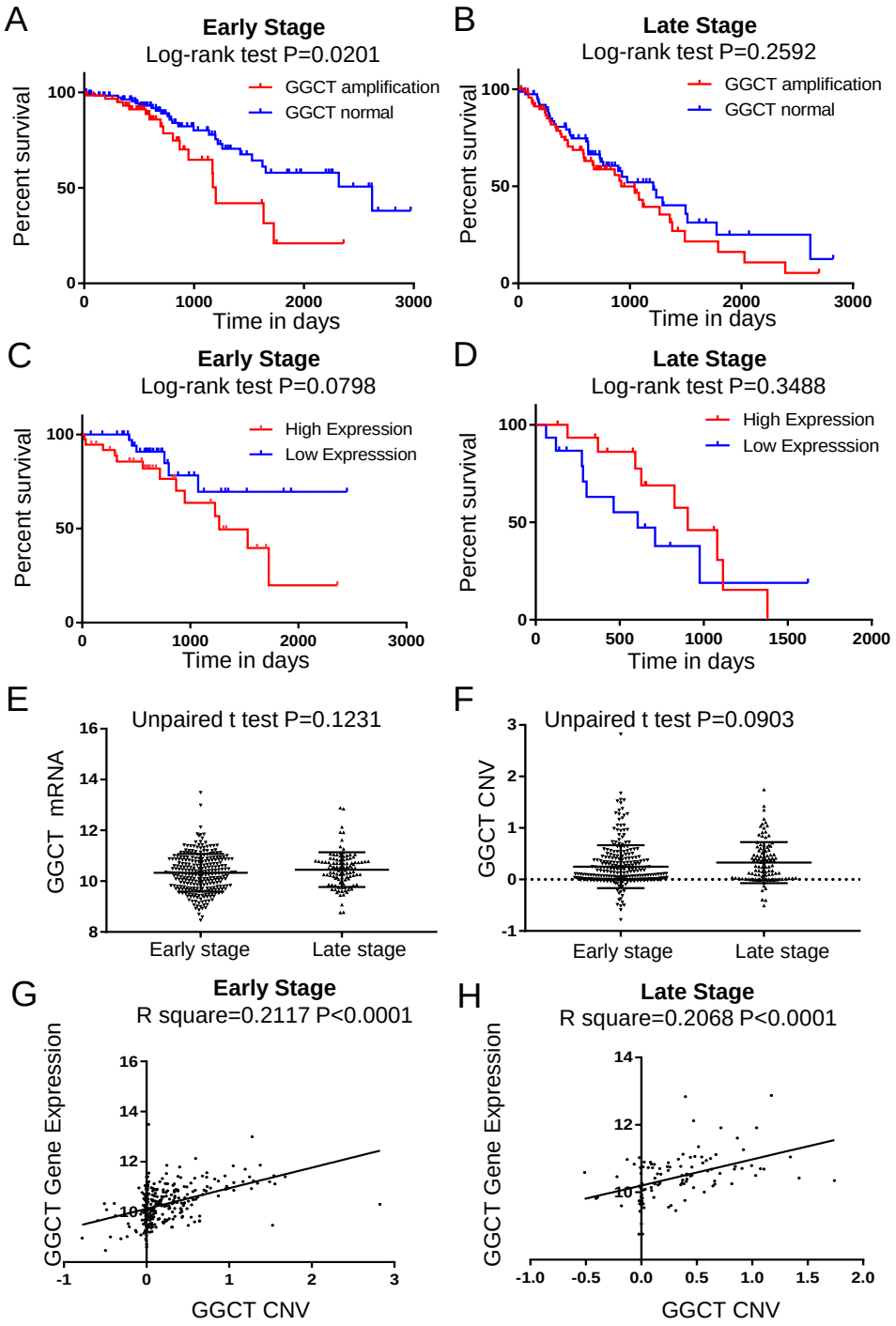

Figure S4. *GGCT* CNV and mRNA up-regulation are associated with poor prognosis in early stage LUAD patients, Related to Figure 2.

(A-D) Kaplan–Meier overall survival curve of LUAD patients are shown. (A and B) Patients are separated into two groups based on *GGCT* CNV value in early stage (A) and late stage (B) LUAD patients. For early stage LUAD, *GGCT* amplification cases contain 60 samples, GGCT no amplification cases contain 114 samples. For late stage LUAD, *GGCT* amplification cases contain 71 samples, *GGCT* no amplification cases contain 78 samples. (C and D) Patients are grouped based on *GGCT* mRNA expression in early stage (C) and late stage (D) lung adenocarcinoma samples. For early stage LUAD, *GGCT* mRNA high expression cases contain 37 samples, *GGCT* mRNA low expression cases contain 40 samples. For late stage LUAD, *GGCT* mRNA high expression cases contain 16 samples, *GGCT* mRNA low expression cases contain 15 samples. Overall survival data was based on TCGA database. Log-rank (Mantel-Cox) test *P* values are shown.
(E and F) *GGCT* CNV (E) and mRNA expression (F) in early stage (n=273) and late stage (n=108) LUAD. (G and H) Correlation between *GGCT* CNV and GGCT mRNA in early stage (n=273) (G) and late stage (n=108) (H) LUAD. Unpaired two-tailed t-test *P* values are shown.

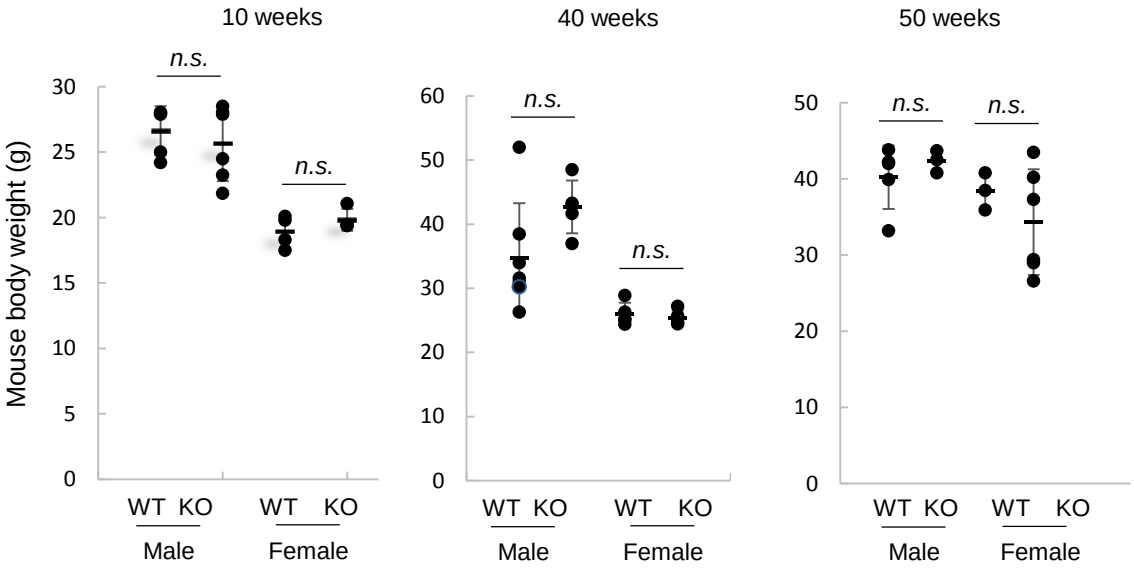

Figure S5. Body weight comparison between *GGCT*$^{+/+}$ and *GGCT*$^{-/-}$ mouse with different ages and sexes, Related to Figure 3.
Male and female *GGCT*$^{+/+}$ (WT) and *GGCT*$^{-/-}$ (KO) mice with different ages are weighted. No significant difference in body weight was observed between *GGCT*$^{+/+}$ and *GGCT*$^{-/-}$ mice.

GGCT$^{-/-}$ vs *GGCT*$^{+/+}$ Primary mouse embryonic fibroblast (MEF)

NAME	NES	NOM p-val	FDR q-val
RB_P107_DN.V1_UP	1.818616	0	0.00479045
E2F1_UP.V1_UP	1.654685	0	0.01618793
GCNP_SHH_UP_LATE.V1_UP	1.564756	0	0.03341101
CSR_LATE_UP.V1_UP	1.476662	0.0039683	0.0574507
HOXA9_DN.V1_DN	1.448844	0.0042553	0.06001841
PRC2_EZH2_UP.V1_UP	1.382798	0	0.09520087
VEGF_A_UP.V1_DN	1.379151	0.0046512	0.08549963
CSR_LATE_UP.V1_DN	1.322314	0.0114504	0.12935296
RPS14_DN.V1_DN	1.310583	0.0080972	0.12997662
ERB2_UP.V1_DN	1.298516	0.0211864	0.13474381

GGCT$^{-/-}$ vs *GGCT*$^{+/+}$ KRAS^{G12D} expressing MEF

NAME	NES	NOM p-val	FDR q-val
RB_P107_DN.V1_UP	1.602945	0	0.172599
CSR_LATE_UP.V1_UP	1.410168	0	0.755149
E2F1_UP.V1_UP	1.336204	0	0.614229
GCNP_SHH_UP_LATE.V1_UP	1.258389	0	1
ERB2_UP.V1_DN	1.216089	0	1
SIRNA_EIF4GI_DN	1.204075	0	1
MEK_UP.V1_DN	1.164132	0	1
VEGF_A_UP.V1_DN	1.160786	0	1
LTE2_UP.V1_DN	1.149189	0	1
HOXA9_DN.V1_DN	1.148979	0	1

GGCT$^{-/-}$ vs *GGCT*$^{+/+}$ Large T antigen expressing MEF

NAME	NES	NOM p-val	FDR q-val
GLI1_UP.V1_UP	1.1033125	0	1
NRL_DN.V1_DN	1.0475771	0	1
SIRNA_EIF4GI_UP	1.0423888	0	1
BCAT_BILD_ET_AL_DN	1.0414152	0	1
CRX_NRL_DN.V1_DN	1.0322751	0	1
CAMP_UP.V1_UP	1.0316353	0	1
ESC_J1_UP_LATE.V1_DN	1.025345	0	1
CSR_LATE_UP.V1_UP	1.0249096	0.169	1
RAF_UP.V1_UP	1.0238483	0	1
PRC1_BMI_UP.V1_DN	1.023609	0	1

Table S3. Differentially expressed gene sets between *GGCT*$^{-/-}$ and *GGCT*$^{+/+}$ MEFs in primary, KRAS^{G12D} expression and large T antigen transformed situations, Related to Figure 4.

Gene set enrichment analysis (GSEA) comparing primary (n=4 for both *GGCT*$^{-/-}$ with *GGCT*$^{+/+}$), *KRAS*^{G12D} expression (n=2 for both *GGCT*$^{-/-}$ with *GGCT*$^{+/+}$), large T antigen transformed (n=2 for both *GGCT*$^{-/-}$ with *GGCT*$^{+/+}$) *GGCT*$^{-/-}$ with *GGCT*$^{+/+}$ MEFs. In each three comparisons, the top 10 enriched gene sets are ranked based on normalized enrichment score (NES) values.

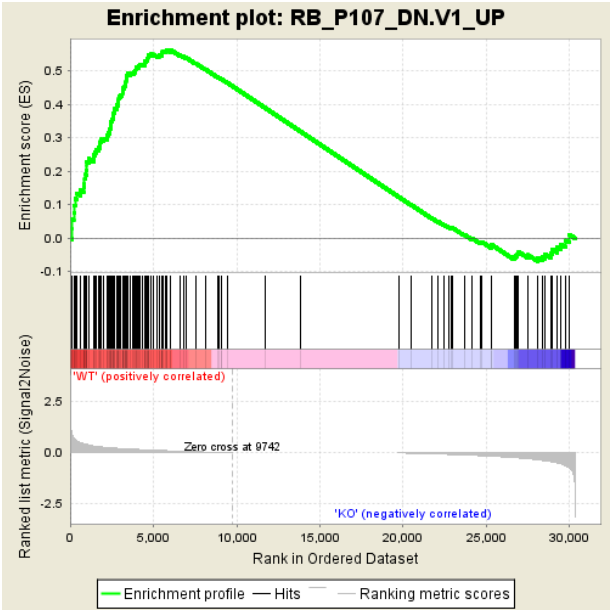

Figure S6. GSEA in primary wild type and *GGCT*$^{-/-}$ MEFs, Related to Figure 4.

RB signature was the top enriched gene signature when compare gene expression difference between wild type and *GGCT*$^{-/-}$ MEFs.

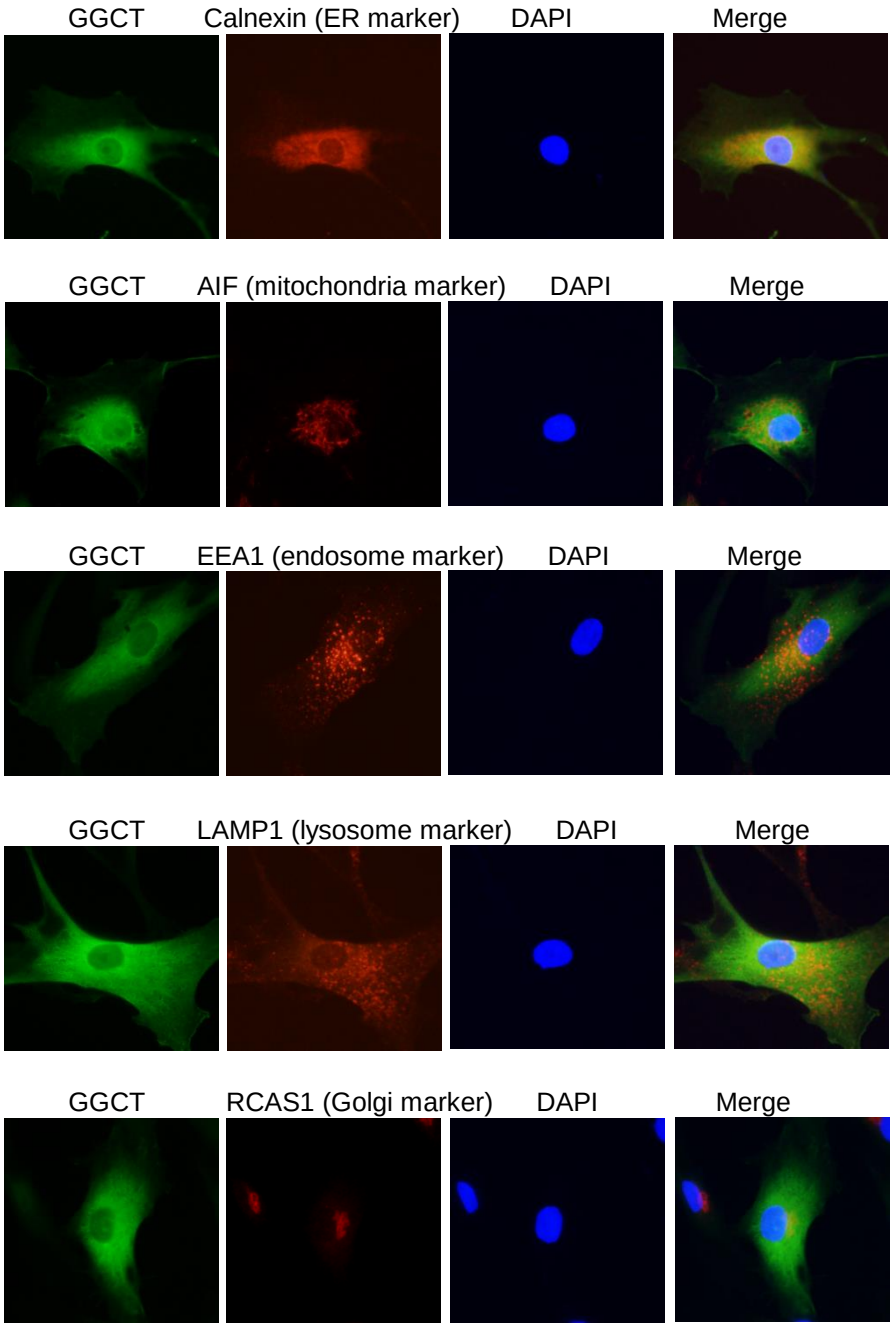

Figure S7. GGCT localization by Immunofluorescence, Related to Figure 6.

FLAG tagged GGCT was stably expressed in human fibroblast, localization of FLAG tagged GGCT was determined with anti-FLAG antibody, and co-stained with various cytoplasmic organelle specific antibodies.

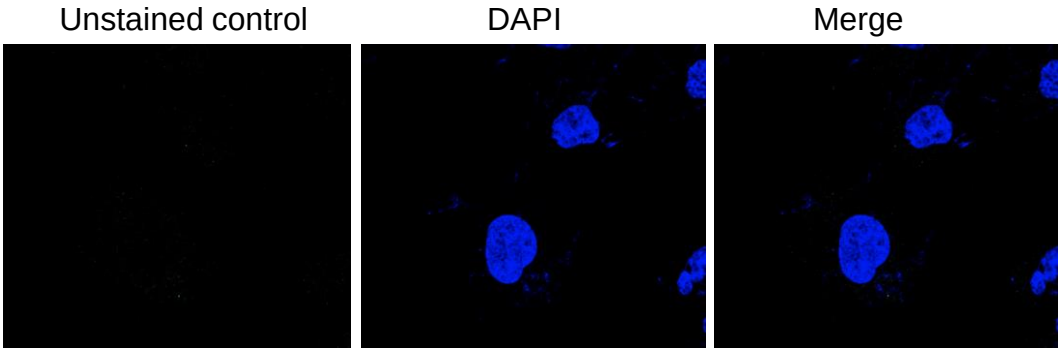

Figure S8. Unstained control for Immunofluorescence, Related to Figure 6.

For immunofluorescence staining, the cells was not stained with FLAG antibody, and no background signals can be detected.

TRANSPARENT METHODS

Antibodies and reagents

Anti-GGCT antibody (ab198503, Abcam), Anti-β-actin antibody (AC-15, Sigma), was used for western blot (WB); Anti-FLAG tag antibody (M2, Sigma), Anti- AIF (D39D2, Cell signaling) antibody (C5C9, Cell signaling), Anti- EEA1 antibody (C45B10, Cell signaling), Anti- LAMP1 antibody (D2D11, Cell signaling), Anti-Calnexin antibody (C5C9, Cell signaling), Anti- RCAS1 antibody (D2B6N, Cell signaling) was used for immunofluorescence; Trametinib (Cayman) was used to inhibit MEK signaling, Carboxy-H2DCFDA (ENZO) was used to measure intracellular ROS level.

Human *GGCT* promoter cloning and luciferase reporter assay

Human *GGCT* promoter containing 677-bp upstream of the transcription start site was amplified from human genomic DNA with the primers.

HuGGCT+105 ATGC AAGCTT CCTGAAGCAGAGTGTAAGGAACGG

HuGGCT-677 ATGC CTCGAG TTAAAAAGAGGAAACGGAGACCAGA

The amplified fragment was cloned into the mammalian expression vector pGL3 basic from Promega using the restriction enzymes HindIII and XhoI (New England Biolabs). Luciferase activity was measured 48 h after transfection with the Dual-Luciferase Reporter Assay System (Promega). Values reported are firefly luciferase divided by Renilla luciferase.

shRNA knockdown and qPCR quantification of gene expression

We performed shRNA experiments with lentivirus vector to knockdown *KRAS* genes in human lung cancer cells. KRAS targeting sequence is “5’-ccggcccgttggagctagtggcgtagttcaagagactacgccactagctccaacttttttggaaa-3’”.

pLKO.1 vectors with *KRAS* targeting shRNA sequence or control sequence (luciferase targeting) was co-transfected with PSPAX2and pMD2G vectors into 293T cells with Lipo2000 transfection reagent according to the manufacturers’ protocol. After 48 h, the culture medium was filtered through a 0.22 μm filter to

obtain retroviral supernatants. Cells were then infected with the retroviral supernatants and 4 μg/ml polybrene, and after 10 h, supernatants were removed and cells were grown with complete growth medium for an additional 24 h. Infected cells were then selected with 1 μg/ml puromycin. After four days of puromycin selection, cells were used for qPCR quantification analyses. The expression of the *KRAS* and *GGCT* genes was examined by quantitative real-time RT- PCR. Total RNA was extracted from cells using TRIZOL reagent and cDNA was synthesized using 1 μg of total RNA with the HiFiScript gDNA Removal cDNA Synthesis Kit. The primer sequences for *KRAS* mRNA quantification were: 5′ - GGACTGGGGAGGGCTTTCT-3′ and 5′ - GCCTGTTTTGTGTCTACTGTTCT -3′. Primer sequences for *GGCT* mRNA quantification were: 5′ -TGGCAATTCCCAAGGCAAAAC-3′ and 5′ - CCCCTTCTTGCTCATCCAGAG -3′.

Gene copy number detection by qPCR

Lung cancer patients' samples and control blood genomic DNA were provided by Feng Zhang of Quzhou People's Hospital, Quzhou, Zhejiang, China. To validate *GGCT* amplification in cell lines and cancer samples, we carried out qPCR using the UltraSYBR Mixture (Cwbiotech) on an ABI 7500 Real-Time PCR system as per manufacturer's instructions. PCR was initiated at 95°C for 10 min, followed by a 40 cycle amplification (95°C 15 sec, 60°C 1 min). Melting curve analysis was performed to ensure specific PCR product while excluding primer dimers. We used the ΔCT method to calculate relative DNA levels normalized to the mean of internal control gene TUBG1, GAPDH and G6PD. PCR primers are listed below.

Gene	sequence(5'to3')
GGCT CNV-F	AGTGACCAGTACCTTTATTCAGCAT
GGCT CNV-R	GCAATACACAACCAGTTAGTGTGAA
GAPDH CNV-F	AGGGAAGCTCAAGGGAGATAAAATT

GAPDH CNV-R	ATCTAAGAGACAAGAGGCAAGAAGG
TUBG1 CNV –F	AATTTGGAAGCCCAGAGTCTAAGAT
TUBG1 CNV –R	GAAGCAGATAAATCTTGATGGCGAA
G6PD CNV – F	CTATCACTGAATCATAAAACCGTGGG
G6PD CNV – R	TCAAAACCTAAGTGTCTGAGCTATCA

Molecular profile data download and processing

mRNA and protein expression data for Lung cancer cell lines were downloaded from the CCLE portal (http://www.broadinstitute.org/ccle/home). LUAD arm-level copy number variation (CNV) data processed by GISTIC2 (Mermel et al., 2011) were downloaded from the Broad firehose database (http://gdac.broadinstitute.org/). *GGCT* mRNA expression, CNV, and clinicopathological data for TCGA cancer types were downloaded from the UCSC Xena database (http://xena.ucsc.edu/) by R package UCSCXenaTools. In total, GGCT expression level of 32 TCGA cancer types and GGCT CNV status of 31 TCGA cancer types were evaluated. There are 15 types of comparable human cancers (both tumor and normal samples available, and the number of normal samples is greater or equal to 10). GGCT expression levels in 14 of 15 cancer types were statistically up-regulated in tumor samples when compared with normal samples. This data and GGCT CNV status for corresponding cancer types are shown in main Figure 2. Copy number profile was measured experimentally using whole genome microarray at a TCGA genome characterization center. Subsequently, GISTIC2 method was applied using the TCGA FIREHOSE pipeline to produce gene-level copy number estimates. GISTIC2 further thresholded the estimated values to -2,-1,0,1,2, representing homozygous deletion, single copy deletion, diploid normal copy, low-level copy number amplification, or high-level copy number amplification. Genes are mapped onto the human genome coordinates using UCSC xena HUGO probeMap. Of note, gene expression was represented as log2(x+1)

transformed RSEM normalized count unless otherwise specified.

Sample classification strategy

To evaluate the influence of CNV status and gene expression status on LUAD prognosis, GISTIC2 estimated value above 0 (representing diploid normal copy) was defined as amplification, and GISTIC2 estimated value equals to 0 was defined as no amplification. For GGCT gene expression, patients with expression value (log2(x+1) transformed RSEM normalized count) at the top/bottom 20% were classified as High/Low Expression group, respectively.

Cell culture

GGCT$^{-/-}$ and sibling control *GGCT*$^{+/+}$ mouse embryonic fibroblasts (MEFs) were isolated from embryonic day 13.5 (E13.5) pregnant *GGCT*$^{+/-}$ female mice mated with *GGCT*$^{+/-}$ male mice. Lung cancer cell lines A549, H1299, H1975 were obtained from ATCC and confirmed to be mycoplasma free. Mouse embryonic fibroblasts (MEFs), 293T cells were cultured in DMEM (Corning, Cellgro) plus 10% Fetal Bovine Serum (FBS) (Gibco), 100 U/ml penicillin G and 100 μg/ml streptomycin (Corning, Cellgro). A549, H1299, H1975 were cultured in RPMI (Corning, Cellgro) plus 10% FBS, 100 U/ml penicillin G and 100 μg/ml streptomycin. All cells were cultured in 37°C, 5% CO2 incubator.

Generation of *GGCT*$^{Flox/Flox}$ and *GGCT*$^{-/-}$ mouse models

GGCT$^{Flox/Flox}$ mouse was generated through ES cell targeting. Targeting vector was based on PGKneoF2L2DTA (addgene plasmid #13445). 5` and 3` arms were amplified from mouse ES cell genomic DNA with the following primers:
5amGgt-USacII, TGCTCTTTTTAGCAGCGCTAGTCC;
5amGgt-DNotI GCTCTAGACTGCTTGCTTTCTCTC;
3amGgt-USalI GTTGTGCGACAGGGTGCCTGATAC;
3amGgt-DEcoRV CTAGATGCAGGATGGCTGGGAGGC;
The replacing exon2 was amplified with following primers:

Exon2Ggt-UXmaI GTGGTATATTGGGATTTAAGGATC;

Exon2Ggt-DSmaI AATTCTACTGTGCTGTTCAATGCC;

The resulting GGCT targeting vector was linearized with SacII and transfected ES cells. The targeted ES clones was initially screened by PCR primers spanning the genomic DNA and inserted cassette, then further confirmed by Sanger sequencing.

Gct5arm-out AGTCATTGCTCTAGACCTTCAGTTT

GGCT5loxp-O GTTCCGGATCCACTAGTTCTAGAGC

Following verification of correct targeting and karyotype, at least two positive ES clones were expanded and injected into blastocysts for mouse generation. The obtained chimeric mouse lines were crossed to C57BL/6J lines for germline transmission. The recombinant founder mice was crossed with ACTB-Flpe mice to get Neo cassette deleted *GGCT*$^{Flox/+}$ mice. *GGCT*$^{Flox/+}$ mice crossed with EIIα-Cre mice to get GGCT$^{+/-}$ mouse. GGCT$^{+/-}$ mouse intercrossed to obtained GGCT$^{-/-}$ mouse. *GGCT*$^{Flox/Flox}$ mice were genotyped with the following primers:

GgctgenoKOFlox-F3a TGAGTCTATGATCTGACAGCAAGAG

GgctgenoFlox-F5a GGAGGGTCACACTTACTAATTGGAT

Predicted PCR product size for wild type allele is 273bp, *GGCT*^{Flox} allele is 449bp.

GGCT$^{-/-}$ mice were genotyped with the following primers:

GgctgenoKOFLOX-F3a TGAGTCTATGATCTGACAGCAAGAG

GgctgenoKO-F5a ATAACCCCTGTGTAACCATCATTCA

Predicted PCR product size for wild type allele is 994bp, *GGCT*$^{-}$ allele is 382bp.

GGCT$^{Flox/Flox}$ and *GGCT*$^{-/-}$ mouse lines were generated by Shanghai Model Organisms Center, Inc. (SMOC). All mouse studies were carried out in strict accordance with the guidelines of the Institutional Animal Care and Use Committee (IACUC) at the School of Life Science and Technology,

ShanghaiTech University.

LSL-Kras G12D mouse model and Adenovirus Cre Administration.

LSL-Kras G12D mouse model was kindly provided by Hongbin Ji of Chinese Academy of Sciences. Both *GGCT*$^{-/-}$ and *LSL-Kras G12D* mice are on C57BL/6 background. 2X10^{8} PFU adenovirus containing Cre recombinase or the control virus was instilled into the lungs of 6 to 8 week old *LSL-Kras G12D* or *GGCT*$^{-/-}$ *LSL-Kras G12D* mice as described previously (DuPage et al., 2009). 12 weeks after adenovirus infection, mouse lungs were inflated and fixed with 4% formaldehyde, then paraffin embedded. Lung sections were stained using haematoxylin and eosin (H&E). Images were taken with Olympus VS120 microscope. H&E sections were statistically analyzed by an operator blinded to genotype. Tumor lesion number was quantified using ImageJ software.

GSH, L-Cysteine quantification by Mass-spectrometry

2X10^{6} cells were seeded in 10cm dishes. 24 hours later, metabolites were extracted with buffer (80% methanol). Samples were dried in a vacuum concentrator, 200 μL extraction liquid (V acetonitrile: V water= 1:1) was added for reconstitution. LC-MS/MS analyses were performed using an UHPLC system (1290, Agilent Technologies) with a UPLC BEH Amide column (1.7 μm 2.1*100mm, Waters) coupled to Triple TOF 6600 (Q-TOF, AB Sciex). The Triple TOF mass spectrometer was used for its ability to acquire MS/MS spectra on an information-dependent basis (IDA) during an LC/MS experiment. MS raw data (.d) files were converted to the mzXML format using ProteoWizard, and processed by R package XCMS (version 3.2). The preprocessing results generated a data matrix that consisted of the retention time (RT), massto-charge ratio (m/z) values, and peak intensity. R package CAMERA was used for peak annotation after XCMS data processing. In-house MS2 database was applied in metabolites identification.

MEFs virus infection

Primary MEFs were infected with *Kras*^{G12D} or Large T expressing retrovirus at passage two. Then selected with puromycin (1 μg/ml for *Kras*^{G12D} retrovirus) or hygromycin (50μg/ml for Large T retrovirus) for three days. The surviving cells after drug selection were harvested for downstream analysis.

Intracellular ROS level quantification by flow cytometry

1.5X 10^5 cells were seeded in each 6 well plate. 24 hour later, Carboxy-H2DCFDA probes (10 μM) was added into culture medium, and cells were stained for 30 min at 37°C. Then staining medium was washed away, the cells were trypsinized, re-suspended and filtered as single-cell solution. Flow cytometry analysis was performed in BD LSR Fortessa Machine. FITC/GFP channel signal was measured. Fluorescent signal data quantification was analysis with FlowJo software.

Immunoblot

Cells were lysed in buffer (50mM Tris, pH8.0, 150mM NaCl and 0.5% NP-40). Protein concentrations of the lysates were measured by Bradford assay. The lysates were then resolved by SDS–PAGE and immunoblotted with the indicated antibodies.

Cell proliferation assay

Cells were seeded in 12-well plates at a density of 10^4/well, then left to grow for four days. Cells were fixed by paraformaldehyde at each time point, and stained with crystal violet. After extensive washing, crystal violet was re-solubilized in 10% acetic acid and quantified at 595 nm as a relative measure of cell number as described previously (Carnero et al., 2000). For serial 3T3 cell proliferation assay, 1.5 X 10^5 cells were seeded into 3.5-cm dishes every 3 days. The cell number was counted with hemocytometer.

RNA-seq analysis

RNA were extracted from primary, *KRAS*^{G12D} or Large T expressing *GGCT*$^{-/-}$ and sibling control *GGCT*$^{+/+}$ MEFs using TRIzol Reagent (Invitrogen, Carlsbad, CA,USA) according to the manufacturer's protocol and then the RNA is quantified by ND1000 Spectrophotometer (NanoDrop Technologies, Wilmington, DE). The cDNA libraries preparation and sequencing were performed by WuXi AppTec according to their standard protocol. Original raw data produced by RNA sequencing were converted to FASTQ files using Illumina CASAVA. We used GSEA (Gene set enrichment analysis) version 3.0 downloaded from Broad Institute to identify the differentially enriched gene signatures between *GGCT*$^{+/+}$ and *GGCT*$^{-/-}$ MEFs. Eight MSigDB gene sets (hallmark gene sets, positional gene sets, curated gene sets, motif gene sets, computational gene sets, GO gene sets, oncogenic signatures, immunologic signatures) were included in our computational analysis. Normalized enrichment scores (NES) were used to rank the differentially enriched gene sets. All RNA-seq data generated in this study has been deposited in NCBI SRA database with the accession number PRJNA554607.

Statistics

The significance of the correlation between *GGCT* CNV, mRNA with clinicopathological characteristics was determined by Student's t-test and fitted with a linear regression model. The significance of the differences between tumor and normal tissues *GGCT* mRNA was tested by unpaired student's t-test assuming unequal sample variance. ANOVA analysis was used when comparing expression levels in more than two groups. Overall survival was estimated using the Kaplan–Meier method with log-rank test. All data were primarily processed by R software (https://www.r-project.org/). Some statistical analyses and visualization were performed using the software GraphPad Prism 7.00 unless otherwise specified. Error bars were presented as means ± SD, and $p < 0.05$ was considered statistically significant.

Supplemental Reference

Carnero, A., Hudson, J.D., Price, C.M., and Beach, D.H. (2000). p16INK4A and p19ARF act in overlapping pathways in cellular immortalization. Nat Cell Biol 2, 148-155.

DuPage, M., Dooley, A.L., and Jacks, T. (2009). Conditional mouse lung cancer models using adenoviral or lentiviral delivery of Cre recombinase. Nat Protoc 4, 1064-1072.

Mermel, C.H., Schumacher, S.E., Hill, B., Meyerson, M.L., Beroukhim ,R., and Getz, G. (2011). GISTIC2.0 facilitates sensitive and confident localization of the targets of focal somatic copy-number alteration in human cancers. Genome Biol. 12, R41.